

Center for Nuclear Waste Regulatory Analyses
Southwest Research Institute

Scientific Notebook No. 1087E

Project No.14010.01.002



Kaushik Das
Debashis Basu

San Antonio, Texas
Phone: (210) 522 4269
Fax: (210) 522 5155
kdas@swri.org



Analytical Support for Regulation of Extended Spent Fuel Storage- Task 2

Team Members

1. K Das
2. D. Basu

Project Number

14010.01.002

Start Date: 20th July; 2011



July 21st 2011

Initial Entries:

The purpose of this notebook is to document the technical activities related to Regulation of Extended Spent Fuel Storage. The main objective will be to assess the internal condition of different casks. Temperature, relative humidity and water content within a canister are of interest to long term integrity of these storage systems. In the present study analytical and computational study will be done to understand the variation of these quantities over time. This notebook will also register and log the document reviews that will be done in this project. This will include previous studies done to assess the internal environment of canister after certain period of storage, open literature related to analytical and numerical study of storage casks, different regulatory guidelines (NUREG) and other associated documents.

~~Account Number: 16607.01.002~~

Corrected Account No. 14010.01.002 Kaushik Das Date 5/13/2013

Software

1. ANSYS-FLUENT 12.1 Software developed by Fluent Inc and currently developed and maintained by ANSYS Inc as a general purpose CFD tool
2. ANSYS-CFX 12.1 A tool similar to ANSYS-Fluent that was developed by AEA technologies and currently developed and maintained by ANSYS-Inc
3. ANSYS-Design Modeler 12.1 Creating the solid geometry necessary for the modeling
4. ANSYS-Meshing 12.1: Mesh generator that discretizes the domain.
5. Tecplot-360 For plotting two dimensional (2D) and three dimensional (3D) data. It was not used for any scientific calculation
6. Intel FORTRAN compiler IFORT for compiling the scripts
7. Microsoft EXCEL Used for basic calculations and plotting

Tasks

1. Perform literature review to obtain suitable cask configuration and dimensions that can be used for the studying the internal environment of a canister.
2. Find suitable correlations or expressions that provide a method for calculating temperature distribution within a canister.
3. Analytically calculate the temperature distribution within a canister.
4. Analytically calculate the relative humidity and water content profile within a canister.



July 26th 2011

Review of Cask Demonstration Project Document and Finding Cask Configuration

Parts of two documents were reviewed as a part of this task to understand the present-state-of-the-art of the cask demonstration projects. It was also done to get an idea about the casks that were used over time for experimentation for cask demonstration work. The following documents were reviewed.

1. Dry Cask Storage Characterization Project 1002882 Final Report, September 2002, Electric Power Research Institute (EPRI) Palo Alto California
2. Materials Aging Issues and Aging Management for Extended Storage and Transportation of Spent Nuclear Fuel, R.L. Sindelar, Principal Investigator A.J. Duncan, M.E. Dupont, P.-S. Lam, M.R. Louthan, Jr., and T.E. Skidmore, Savannah River National Laboratory Aiken, SC 29808, R.E. Einziger, NRC Technical Project Manager Date Published: May 2011

Some other associated documents were also studied to understand the historical context of this study and look at some of the temperature data that was recorded at the earlier phase of the study. Some of the documents are

1. Dry Cask Storage Characterization Project- Phase I: CASTOR V/21 Cask Opening And Examination, W. C. Bare and L. D. Torgerson, August 2001, Idaho National Engineering and Environmental Laboratory Idaho Falls, Idaho 83415
2. Spent Nuclear Fuel Integrity During Dry Storage, M.A. McKinnon, I. Stewart IAEA-SM-352/37
3. Spent Nuclear Fuel Storage – Performance Tests And Demonstrations, M.A. McKinnon and V A DeLoach, PNNL-8451, UC-510, Pacific Northwest Laboratory Richland, Washington 99352
4. Spent Fuel Integrity During Dry Storage, M McKinnon, Institute of Nuclear Materials Management 36th Annual Meeting July 9-12, 1995 Palm Desert, California
5. Spent Nuclear Fuel Integrity During Dry Storage-Performance Tests and Demonstration, McKinnon and Doherty, PNNL-11576 and UC-810, June 1997, Pacific Northwest National Laboratory

A number of casks were studied in this program that included both canister based and direct loaded systems. The following casks were studied.

1. REA-2023 (Ridihalgh, Eggers & Associates and later available from Mitsubishi Heavy Industries ,Ltd)
2. GSN Castor V-21 (Gesellschaftfur Nuklear Service, GSN)
3. TN-24P (TransNuclear and presently AREVA)
4. MC-10 (Westinghouse)



5. VSC-17 (Sierra Nuclear Corporation)
6. NUHOMS (NUTECH horizontal modular storage system, later TransNuclear and presently AREVA))

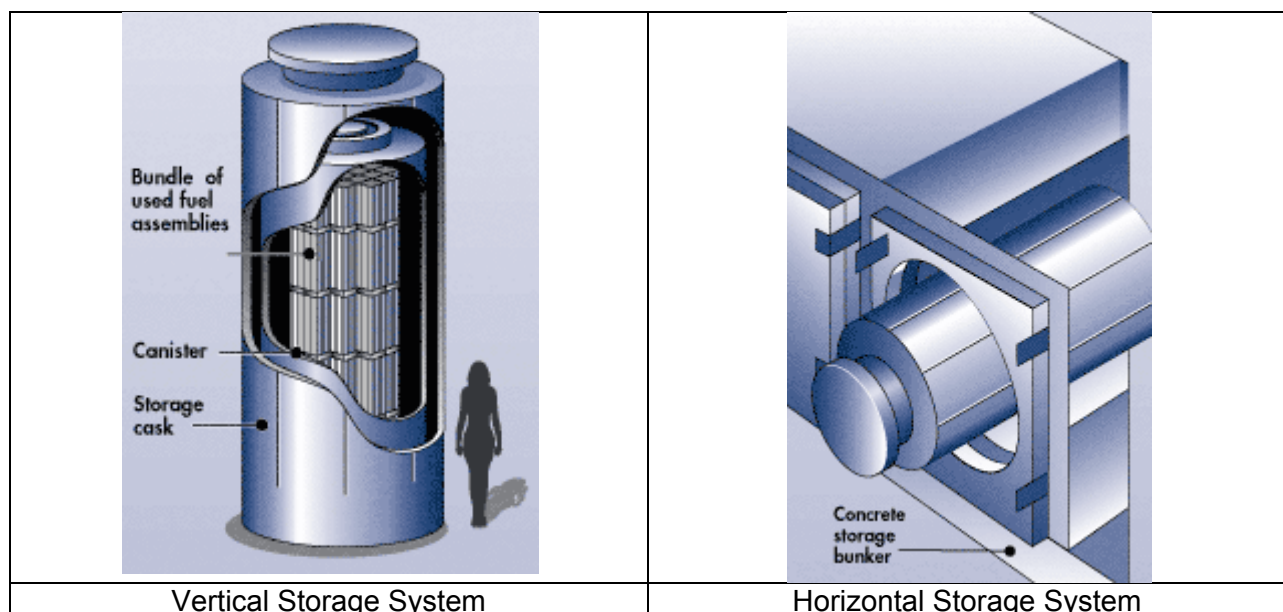
The temperature profiles and other quantities of interest were provided in the reports by McKinnon (Spent Nuclear Fuel Integrity During Dry Storage, M.A. McKinnon, I. Stewart IAEA-SM-352/37. Some of it will be used in the present study.

Factors That Affect Cask Component And Cask Internal Temperature

1. Cask geometry
2. Backfill gas (Helium/Nitrogen) or the vacuum condition; More than the temperature, it will affect the distribution of temperature along the fuel rod.
3. Fuel characteristics
 - a. Burnup
 - b. Peaking factor profile\

This is possibly the most important factor affecting the cask internal temperature
4. Component of interest
 - a. Location
 - b. Specific component thermal property

The following figures are used to show some relative dimension and components of a typical dry storage cask





July 28th 2011

Selection of a Representative Cask

The temperature and relative humidity distribution will likely vary significantly from a design of cask to another as the geometry and components will differ in size, shape, orientation and material property. The cask geometry is perhaps the second most important factor after fuel a characteristic that significantly affects temperature and relative humidity distribution. Selection of a representative cask is important as a baseline is required to initiate the study of relative humidity and temperature.

Basis of selection

The following factors has to be kept in mind while trying to select a cask for the present study

1. Available dimensions
2. Known fuel characteristics
3. Experimental Data
4. Known material of construction (this has to be available either from the manufacturer or from handbooks if standard non-proprietary material has been used)

The GNS CASTOR V-21 cask that has been studied by EPRI for the extended storage cask demonstration project will initially be used for baseline study in the proposed activity. It may, however, be required that we study a different cask later that is more amenable to test certain other objective. But presently the CASTOR cask seems to satisfy most of the requirement mentioned above.

This is direct load cask and not a canisterized system and can be opened by opening the bolts to study the cask internals

Some notes about the CASTOR V-21 cask

1. Cast Iron Cask for Storage and Transportation
2. Gesellschaft für Nuklear-Service mbH (GNS)
3. Studied Extensively at INL and ANL

Cask Body

Detailed description of the body is available in the EPRI cask demonstration report. Here some important highlights are mentioned

- Single Cylindrical Structure
- 8 ft External Diameter
- 16 ft High
- 73 Heat Transfer Fins



- PE Moderator Rods

This figure may be copyrighted therefore is not included in the notebook. Reference Figure 1-1 from Electric Power Research Institute, "Dry Cask Storage Characterization Project", Final Report, Report Number 1002882 September, 2002, EPRI, Palo Alto, California

Representative Diagram of the CASTOR V-21 cask EPRI 2002

Spent Fuel Basket

- 21 Fuel Tubes
- 13.5 ft High
- Shrink Fit with Cavity Inner Surface

The CASTOR V-21 cask has a primary and secondary lead, but the secondary lead was not used due to placement of different probes and for ease of monitoring. This will alter the thermal characteristics, but the alteration will be insignificant.



This figure may be copyrighted therefore is not included in this notebook. Reference Figure 1-2 from Electric Power Research Institute, "Dry Cask Storage Characterization Project", Final Report, Report Number 1002882 September, 2002, EPRI, Palo Alto, California

Horizontal Sectional View of CASTOR V/21 EPRI 2001

This figure may be copyrighted therefore is not included in this notebook. Reference Figure 1-3 from Electric Power Research Institute, "Dry Cask Storage Characterization Project", Final Report, Report Number 1002882 September, 2002, EPRI, Palo Alto, California

Schematic of Primary Lid EPRI 2002

August 5th 2011

This figure may be copyrighted therefore is not included in this notebook. Reference Figure 2-22 (Top) from Electric Power Research Institute, "Dry Cask Storage Characterization Project", Final Report, Report Number 1002882 September, 2002, EPRI, Palo Alto, California

15×15 Fuel Assembly that was Used in CASTOR V-21 EPRI 2002



This figure may be copyrighted therefore is not included in this notebook. Reference Figure 2-22(bottom) from Electric Power Research Institute, "Dry Cask Storage Characterization Project", Final Report, Report Number 1002882 September, 2002, EPRI, Palo Alto, California

Fuel Arrangement Within an Assembly and Other Associated Components Holding The Assembly EPRI 2002

Fuel Characteristics

As mentioned, the fuel characteristics are perhaps the most important factor that affects the temperature and fuel characteristics of the cask system. The Westinghouse PWR fuel was used to study the CASTOR V-21 cask. The following highlights some points to be noted about the fuel

- Fuel assembly originated from dominion powers surrey reactor
- Westinghouse PWR fuel
- 15×15 fuel assembly
- Assembly t11 (shown in the following figure) was instrumented and studied
- Assembly average burnup of 35.7 gwd/mtu
- Discharged in November 1981
- Loaded on cask in July 1985
- Average decay heat on loading 1.1 KW per assembly

Temperature Measurement

Two sets of temperature measurements were taken

The first sets of measurements were obtained in 1985. Thermocouple Lance System was used to take measurement with primary lid on. Hence a detailed temperature measurement was recorded with spatial variation along the fuel basket and liner.

The second set of temperature measurements were recorded in year 1999 (after 14 years) with only isolated thermocouples, but no lances. As a result, temperature measurements at isolated locations, were recorded. Spatial distribution of temperature field in 1999 was not recorded.



Moreover, in 1999, the primary lid was completely removed and the fuel arrangement was exposed to atmosphere. As a result it is expected that the measured temperature was lower than what would actually be experienced within a closed cask

This figure may be copyrighted therefore is not included in this notebook. Reference Figure 2-16 from Electric Power Research Institute, "Dry Cask Storage Characterization Project", Final Report, Report Number 1002882 September, 2002, EPRI, Palo Alto, California

Fuel Assembly Nomenclature McKinnon 1997

August 10th 2011

Peak Temperature Values

Peak Temperature in Fuel Assembly

- 1985: 358° C
- 1999: 155° C

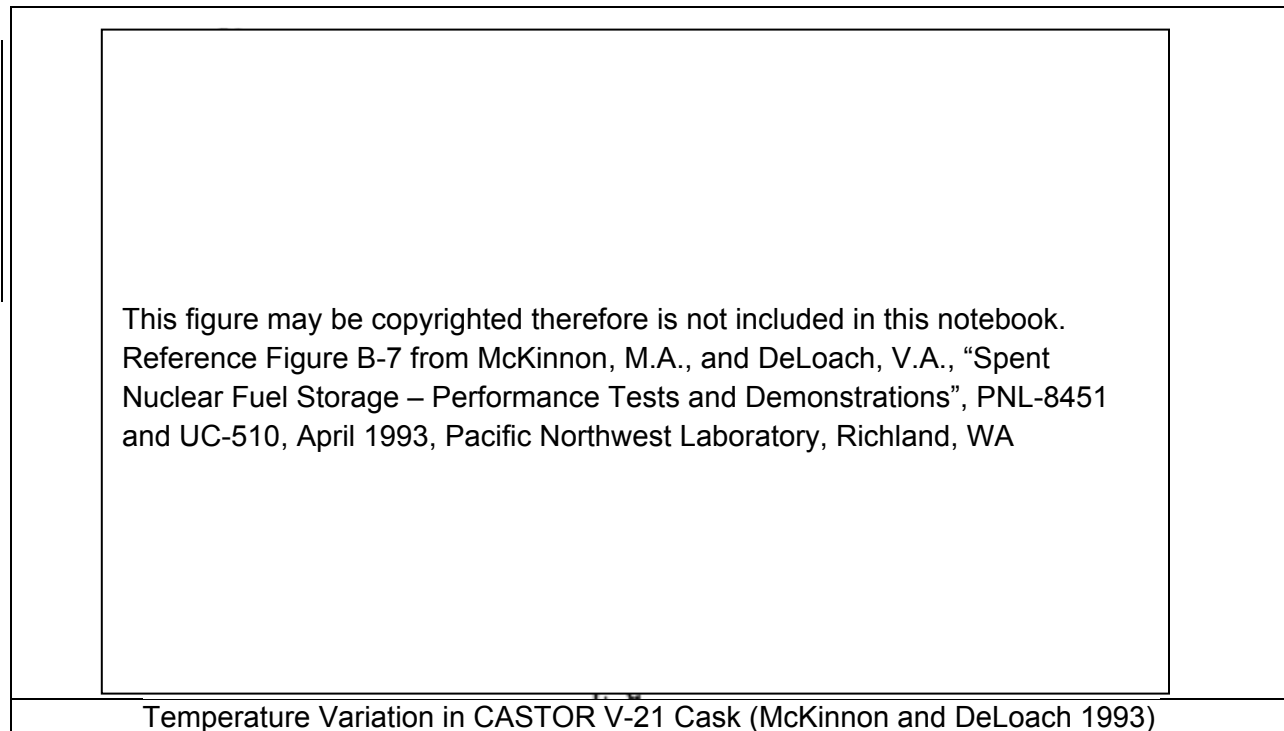
Peak Temperature in External Surface

- 1985: 105.3° C



- 1999: 60.6° C

Spatial distribution of the temperature is provided in the figure below



August 11th 2011

Empirical Correlation for Estimating Temperature Distribution over Time

Empirical correlations for calculating temperature distribution over time were done at the Argonne National Laboratory by Einziger et. al. The procedure is described in the EPRI report on cask demonstration report. The method is described in Part-2, section 2.1.2. In this work, an upper and lower bound of temperature was computed.

The lower bound calculation

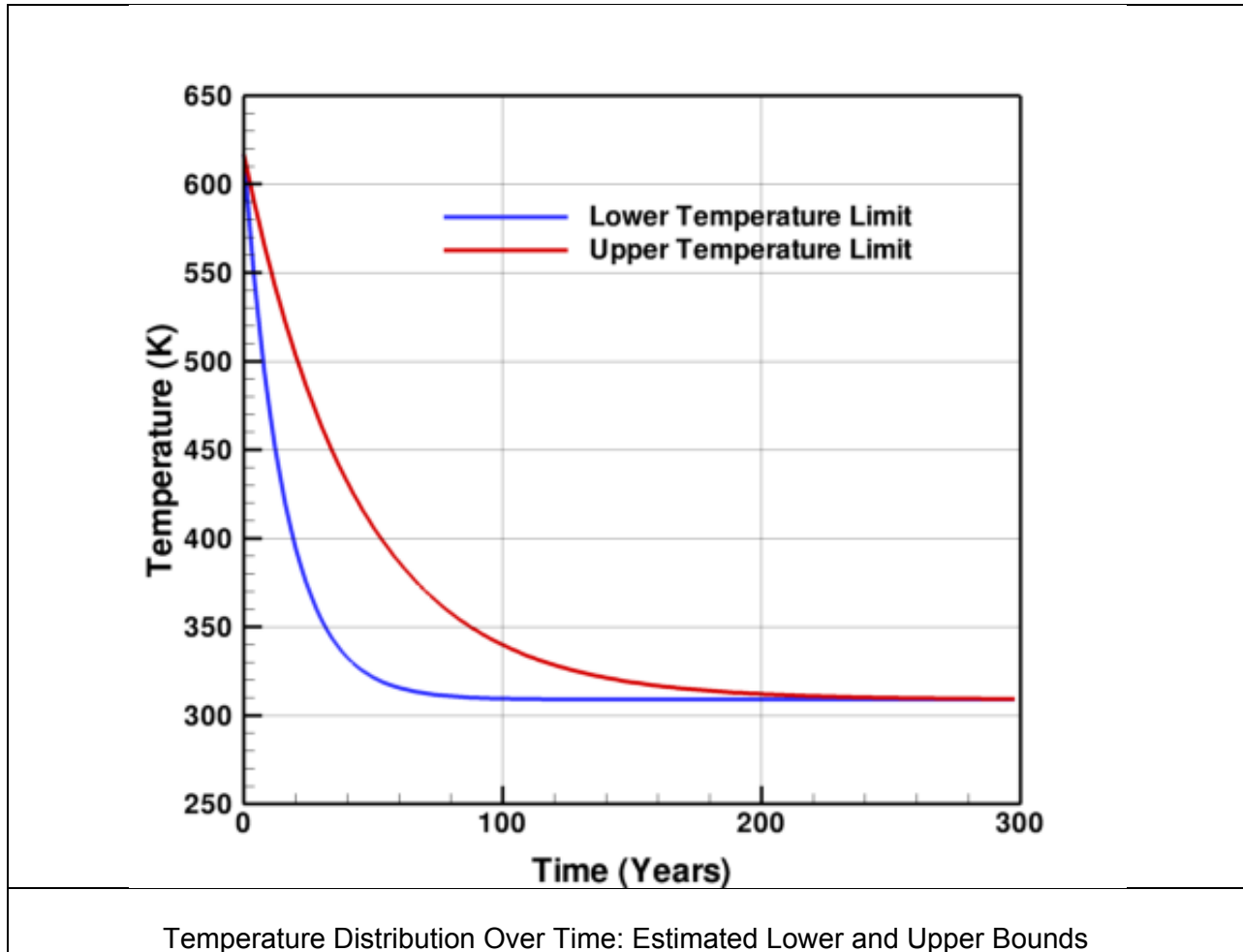
The following assumptions were made for the lower bound of temperature calculations

1. Initial Temperature : 617 K (start of extended storage)
2. At 14.8 years, temperature of 428 K (when the cask was opened)



3. At 100 years, the ambient temperature of 38°C, will occur
Using these assumptions, the following equation was obtained, that provided the lower bound of temperature for the CASTOR V-21 cask.

$$T(t) = 308 \exp(-0.064 t) + 309$$



The upper bound calculation

The upper bound was calculated using the following assumptions

1. Temperature would be proportional to the exponentially decreasing decay heat until eventually the ambient temperature dominated.
2. Main sources of decay heat are Cs-137 and Sr-90, but as their half lives are close, the half life of Cs was used in the calculation.
3. The initial temperature was assumed to be 344°C



4. The final temperature was set to be at the ambient condition, which is equal to 38°C
The following equation was derived based on these assumptions

$$T(t) = 308 \exp(-0.023 t) + 309$$

The temperature distribution obtained the lower and upper estimates are shown in the last figure

August 12th 2011

Relative Humidity Calculation

Relative humidity was calculated based on the following assumptions

1. Open Volume fixed at 7 m³
This assumption is subject to further verification of geometrical configuration of the system and will influence the final calculation, since the volume is directly linked with the partial pressure of water
2. Uniform Condition within Open Space
 - a. Lumped Parameter Assumption
 - b. Spatial Distribution Not Considered
This essentially means that we are considering a point formulation that is representative of the system. No spatial variation takes place and the volume within the canister is treated like a lumped system
3. Condensation Starts at Saturation Condition
Condensation of water will only take place when the representative point mentioned above reaches the saturation condition, In reality, there will be spatial variation in condensate formation within the system and some places will start getting moisture cover before other, depending on local temperature
4. Quantity of Water Vapor Does Not Affect Pressure Distribution
 - a. Pressure remains the same after Condensation
This essentially means that the water vapor only exerts a minor fraction of the total pressure and the mass of water vapor is insignificant. This may need further revision if there is a significant quantity of water.
5. Latent Heat Exchange with Solid Surfaces Only
 - a. Gas Temperature not affected by Condensation, as the phase change heat transfer takes place only at the wall. This is a reasonable assumption as the thermal mass of the wall is higher compared to the gas mass.
6. Ignores Other Physical/Chemical Processes
 - a. This implies that water consumed due to corrosion is not accounted for in the inventory



- b. If there is any other chemical reaction taking place such as radiolysis that can potentially affect water inventory, it is neglected.
- c. Presence of any fission gas due to cladding failure is not accounted for in the system

Relative Humidity Calculation Method

The following equation is used to calculate relative humidity (RH)

$$RH = 100 \times \frac{P_{vp}(T)}{P_{vp,sat}(T)}$$

where

$P_{vp}(T)$ Partial pressure of water vapor at the temperature (T)
 $P_{vp,sat}(T)$ Saturation vapor pressure of water vapor at the temperature (T)

The temperature value T could be obtained as a function of time based on the upper and lower bounds described in the previous section

The saturation vapor pressure as a function of temperature can be obtained using the following relationship

$$P_{v,sat}(T_C) = 217.99 * \exp \left[\frac{0.01}{273.15 + T_C} (374.136 - T_C) \sum_{k=0}^7 F_k (0.65 - 0.01T_C)^k \right]$$

where $P_{v,sat}$ = water vapor saturation pressure in atm

TC = temperature in °C

| | |
|----------------|-----------------|
| F0 = -741.9242 | F1 = -29.721 |
| F2 = -11.55286 | F3 = -0.8685635 |
| F4 = 0.1094098 | F5 = 0.439993 |
| F6 = 0.2520658 | F7 = 0.05218684 |

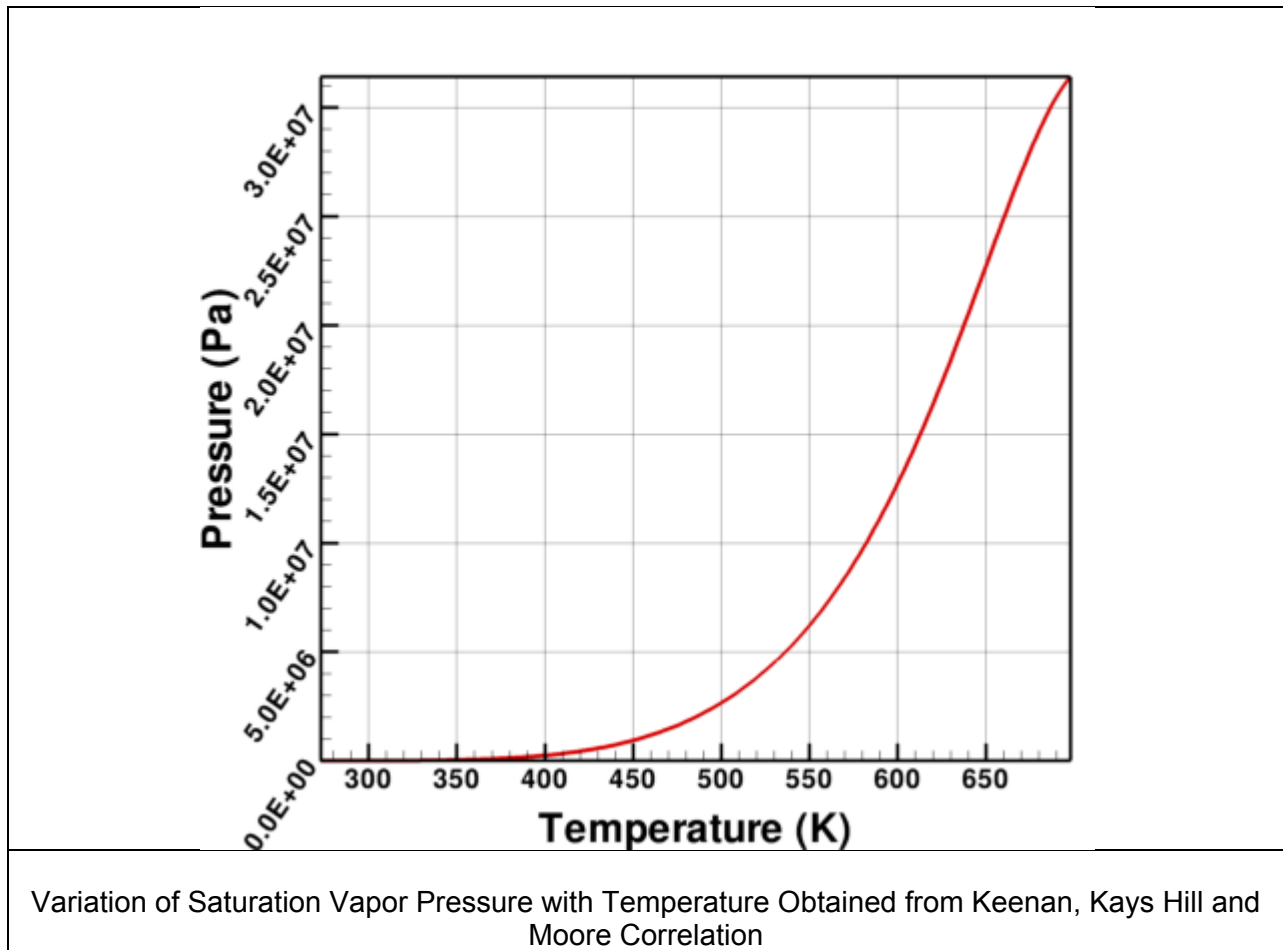
Reference:

Keenan, J. H., Keyes, F. G., Hill, P. G., Moore, J. G., Steam Tables: Thermodynamic Properties of Water, Including Vapor, Liquid, and Solid Phases, John Wiley and Sons, Inc, 1969. As cited in Chapter 5 of ASHRAE Handbook and Product Directory, 1977 Fundamentals, Third Printing,



American Society of Heating Refrigeration and Air Conditioning Engineers, Inc., New York, p. 5.12.

The temperature range of validity for the above mentioned equation is 0°C to 374°C. The main reason for choosing this relationship is that it is valid for the temperature range that is expected in a normally functioning cask over time. The primary interest is the temperature range when condensation is likely to happen, which is within the validity limit of the cask system.





August 17th 2011

Another correlation that covers the temperature range of interest is the Keenan-Keeyes Formula. This is valid for the temperature range of 10°C to 150°C. Though the cask will experience higher temperature values, it is extremely unlikely that condensation will take place above 150°C within the cask. However that is dependent on the cask internal pressure

$$\log_{10}\left(\frac{P_{v,sat}}{218.167}\right) = \frac{\beta}{T} \left(\frac{a + b\beta + c\beta^3}{1 + d\beta} \right)$$

where

$$a = 3.2437814$$

$$b = 5.868276 \times 10^{-3}$$

$$c = 1.1702379 \times 10^{-8}$$

$$d = 2.1878462 \times 10^{-3}$$

$$\beta = 647.27 - T$$

T = absolute temperature, Kelvin

$P_{v,sat}$ = water liquid - vapor saturation pressure, atmospheres

Reference

Keenan, J. H., and Keyes, F. G., Hill, P. G., Moore, J. G., Thermodynamic Properties of Steam, John Wiley and Sons, Inc, 1936, p. 14. As cited in Chapter 5 of ASHRAE Handbook and Product Directory, 1977 Fundamentals, Third Printing, American Society of Heating Refrigeration and Air Conditioning Engineers, Inc., New York, p. 5.12.



Calculation of Condensate Mass

At any point of time, the condensate mass was calculated using the following equation

$$n_{cond}(t) = n(t) - n_{sat}(T)$$

Where,

$n_{cond}(t)$

Amount of condensate water mass at time t in moles

$n(t)$

Amount of water vapor at that point of time (t) in moles

$n_{sat}(T)$

Saturation mole fraction at temperature T

$$n_{sat}(T) = \frac{P_{vp,sat}(T) \times V}{RT}$$

The term $n_{sat}(T)$ calculates the number of moles of water vapor in saturation condition at temperature T. Any water present in excess to that will have to be condensed in order to maintain equilibrium. The equations above will an idea about the water vapor remaining in the system. Once it reaches the saturation limit, the water vapor content will remain at the saturation value.

The equations above were codes in a simple FORTARN program described below



c Relative Humidity Calculation

c*****

```
real rgas ! gas constant
real nw_h ! Number of moles of water high temperature
real nw_l ! Number of moles of water low temperature
real nw_ini ! Number of moles of water initially present
real nw_sat
real nw_cond
real MW_water
```

```
dimension nw_h(5000)
dimension nw_l(5000)
```

```
nw_ini = 54.0
vol = 7.0 ! Open volume within the cask
rgas = 8.314 ! R in J/K-mole
MW_water = 18.0/1000. !Molar weight of water kg/mole
```

```
dt = 2.0 ! Time step size in years
t0 = 0.0 ! Start Time
tf = 300.0 ! End time
N = ifix((tf-t0)/dt) ! Number of time steps
write(*,*) 'Time step size in years=',dt
write(*,*) 'End time=',tf
write(*,*) 'Number of time steps=',N
```

```
open(unit=20,file='temp-humidity.dat')
open(unit=21,file='sat-pressure.dat')
write(20,*) 'Title=Temperature-Humidity-Data'
write(20,*) 'variables=Time,Temperature,Relative Humidity,
& Water-content,Condensed-water-moles,Condensed-water-kg'
```

c Upper temperature limit loop

```
write(20,*) 'zone T= "Upper Limit", i=',N,',f=point'
nw_h(1) = nw_ini
do i=1,N
time= t0+ dt*(float(i-1)) ! Time in years
temp = 308.0*exp(-0.064*time)+309 ! Temperature in K
pvp = nw_h(i)*rgas*temp/vol ! Partial pressure of wv
psat = fpsat(temp) ! Saturation Vapor Pressure
write(*,*) 'temp=',temp,' pvp=',pvp,' psat= ',psat
rh = pvp*100.0/psat
if (rh.gt.100.0) then
rh = 100.0
nw_sat = psat*vol/(rgas*temp)
nw_cond = nw_h(i) - nw_sat
else
nw_cond = 0.0
endif
nw_h(i+1) = nw_h(i)-nw_cond
w_cond = nw_cond*MW_water
write(20,*) time,temp,rh,nw_h(i),nw_cond,w_cond
enddo
```

```
c do i=1,N
c time= t0+ dt*(float(i-1)) ! Time in years
```



```

c      temp_h = 308.0*exp(-0.064*time)+309      ! Temperature in K
c      temp_l = 308.0*exp(-0.023*time)+309      ! Temperature in K
c      pvp_h = nw*rgas*temp_h/vol              ! Partial pressure of WV
c      pvp_l = nw*rgas*temp_l/vol              ! Partial pressure of WV
c      psat_h = psat(temp_h)
c      psat_l = psat(temp_l)
c      rh_h = pvp_h*100.0/psat_h
c      rh_l = pvp_l*100.0/psat_l
c
c      if (rh_h.gt.100.0) then
c          rh_h = 100.0
c          nw_sat = psat_h*vol/(rgas*temp_h)
c          nw_cond = nw - nw_sat
c
c      write(20,*) time,temp_l,temp_h,rh_h,rh_l
c      write(21,*) temp_h,psat_h
c      write(*,*) time,temp_l,temp_h,i
c
c      enddo
c
close(20)
stop
end

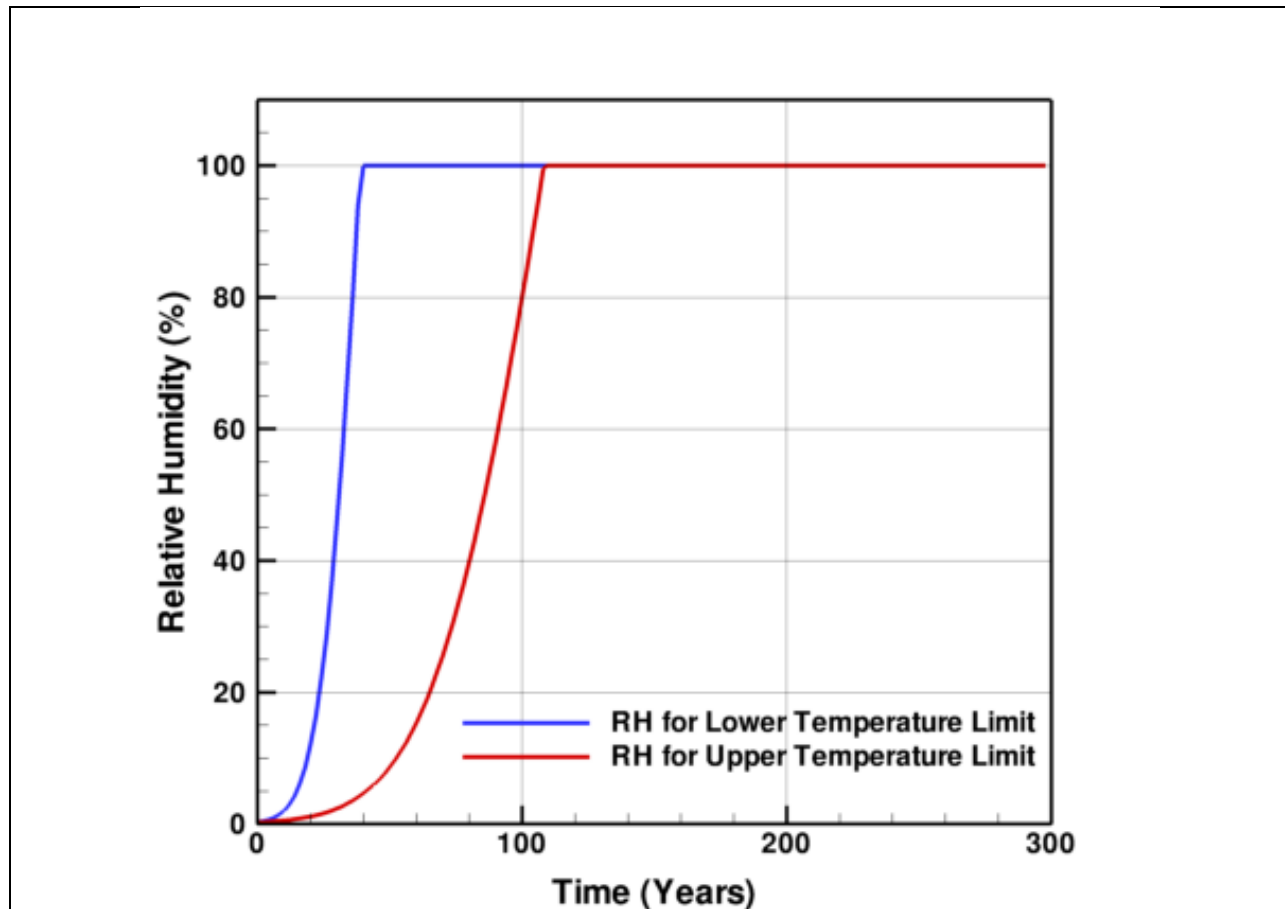
function fpsat(temp2)
dimension f(8)
f(1)=-741.9242
f(2)=-29.721
f(3)=-11.55286
f(4)=-0.8685635
f(5)=0.1094098
f(6)=0.439993
f(7)=0.2520658
f(8)=0.005218684
tc=temp2-273.0 ! Temperature in deg C
total=0.0
do i= 1,8
    total = total + f(i)*((0.65-0.01*tc)**(i-1))
enddo
term=0.01*(374.136-tc)/(273.15+tc)
psat=101325.0*217.99*exp(term*total)
return
end

```

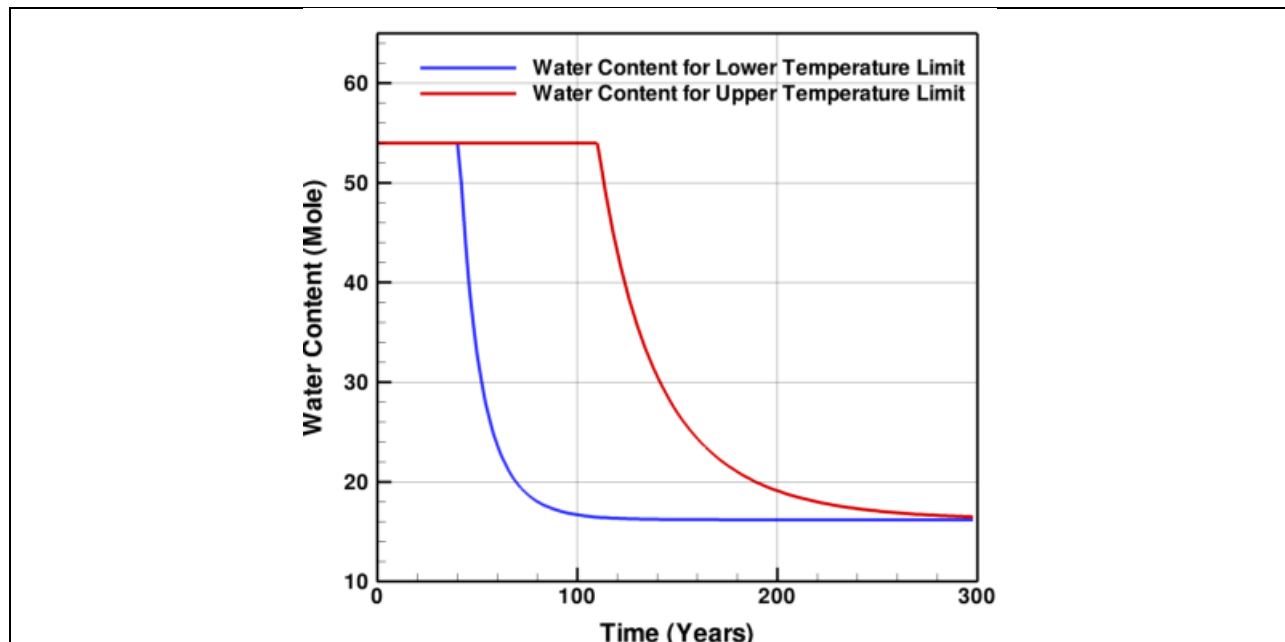


August 26th 2011

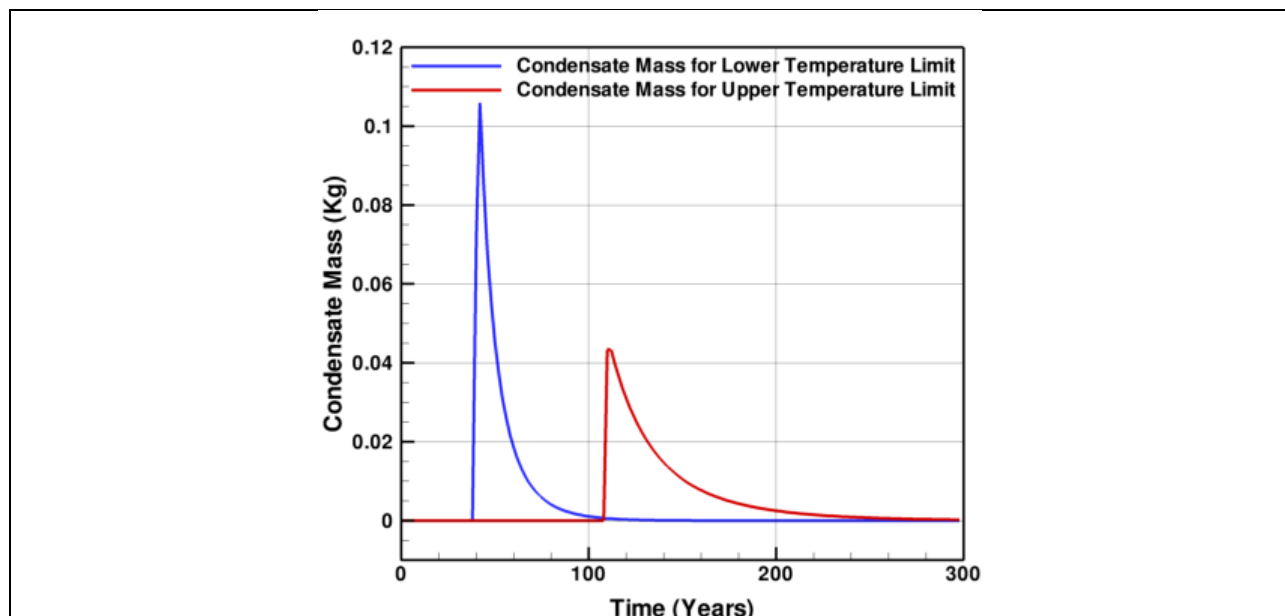
Relative Humidity Distribution



This figure shows the relative humidity distribution for the high and low temperature limits and was calculated using equations described in previous section. As can be seen that the lower temperature limit hits the 100% limit faster than the high temperature limit estimation. This is obvious as the relative humidity calculation uses a point approach and the low temperature estimate reaches the saturation condition faster.



This figure shows the water content in the system and its variation with time. As soon as the system reaches an RH of 100%, condensation starts and the gas phase starts losing water mass to liquid phase.



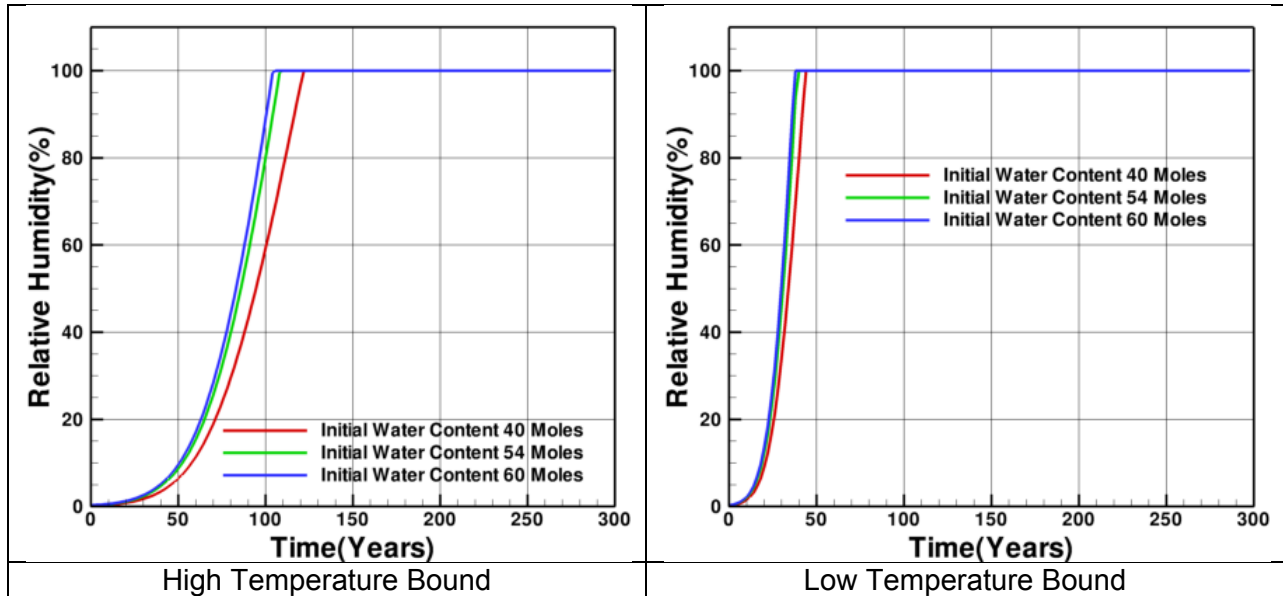
This figure shows the condensation rate. This is complementary to the previous figure and the total condensed mass and the total water vapor mass should sum up to the initial mass of water



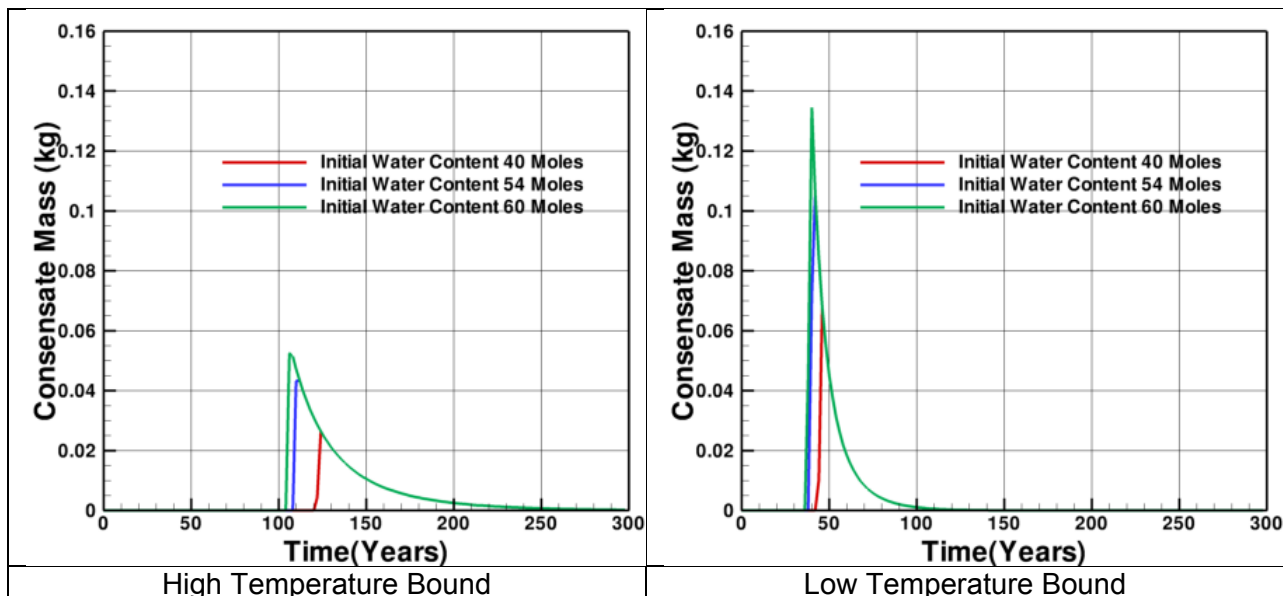
August 29th 2011

Parametric Study to Understand the Effect of Initial Water Vapor Mass

The initial water content was varied and three values were tested (40 moles, 54 moles and 60 moles)



The variation in relative humidity profiles for low and high temperature estimates are shown here. At high water content level, the system reaches saturation faster compared to low water content in the system.





The condensation pattern also reflects the same understanding that systems with higher water content will reach saturation faster and will condense more water. Whereas, the system with initial lower water content will exhibit the opposite pattern. Both the upper and lower temperature bound estimate calculations show the same trend.

Date 10/1/2011

Links to NRC site for licensed cask vendors and cask types

<http://www.nrc.gov/waste/spent-fuel-storage/designs.html>

<http://www.nrc.gov/reading-rm/doc-collections/cfr/part072/part072-0214.html>

Date 11/24/2011

Contents of the Report and Analysis

This chapter will first summarize literature information on temperature-time and temperature spatial profiles inside the cask during extended storage and then provide independent analysis results on temperature-time, temperature spatial, and relative humidity profiles. The temperature and relative humidity window for materials degradation will also be discussed.

Spatial Temperature Distribution of Spent Fuel Storage Systems- spatial profiles during extended storage

Heat transfer in the storage cask is a complex process because of the storage cask geometry and the combined convection and radiation induced by the decay heat of the spent fuel. The specifics of the heat transfer mechanism are dependent on a number of factors that include cask configuration. Presently, two different cask configurations are used to store spent fuel. In the first configuration, spent fuel assemblies are placed within a basket that is loaded into a metal cask. There is no gap between the cask surface and the basket assembly and the cask is closed and sealed using a bolted lid. In this design, the principal mode of heat transfer is through convection at the outermost surface of the cask. In the second configuration, the basket spent fuel assemblies are placed in a basket within a canister that is sealed using a welded lid. The canisterized fuel is subsequently put within a cask, with an annular gap between the outer periphery of the canister and inner periphery of the cask for air circulation. In this configuration, the primary mechanism of heat transfer from the canister is through the natural convection of air flow through the gap, where cooler air enters the air passage near the bottom of the gap, flows



vertically upwards as it absorbs decay heat and the low density hot air exits the system near the top.

Previous Studies

McKinnon and DeLoach [1993] performed detailed experimental study to understand the thermal behavior of six different combinations of cask designs and fuel characteristics. They include (i) Ridihalgh, Eggers & Associates REA 2023 cask with 7×7 BWR fuel assembly (ii) Gesellschaft für Nuklear Service (GNS) CASTOR-V/21 cask with 15×15 PWR fuel assembly (iii) Transnuclear, Inc. TN-24P cask with general 15×15 PWR fuel assembly (iv) Transnuclear, Inc. TN-24P cask with consolidated 15×15 PWR fuel assembly (v) Westinghouse MC-10 cask with 15×15 PWR fuel assembly (vi) NUTECH horizontal modular storage system (NUHOMS) with general 15×15 PWR fuel assembly (vii) Sierra Nuclear Corporation ventilated vertical concrete storage cask (VSC-17) with consolidated 15×15 PWR fuel assembly. The experimental study was conducted for three canister backfill scenarios with Nitrogen and Helium as backfill gas and a near vacuum condition. The experimental data obtained from the study showed spatial temperature variation along different cask components such as the fuel assemblies, outer surface and the fuel basket. In addition to the experimental study, two thermalhydraulic codes, COBRA-SFS [Lomberdo et al. 1986] and HYDRA [McCann and Lowery, 1987] were used to calculate the spatial temperature distribution. This experimental study was the foundation of the subsequent cask demonstration exercise that was subsequently performed at Idaho National Laboratory (INL) and Argonne National Laboratory (ANL). A series of reports (McKinnon, 1997; McKinnon and Doherty, 1997, Bare and Torgerson, 2001, Electric Power Research Institute, 2001) describe subsequent study and progress related to cask demonstration project.

Detail experimental and numerical study of spent nuclear fuel storage systems have been carried out that explored the physics and mechanism of heat dissipation mechanism of such systems. In general, most of the studies have indicated that spent-fuel heat generation rate, thermal boundary condition, canister backfill media, and cask orientation with respect to gravity that dictates natural convection pattern are the major contributing factor in determining the heat transfer and by extension the spatial temperature distribution pattern of a spent fuel storage system. Investigations by Arya and Keyhani, 1990; and Cannan and Klein, 1998 mainly focused on the natural convection pattern within the spent-fuel assemblies. A recent investigation by Heng et al. (2002) found that the dominant heat transfer mode changes from conduction to convection with an increase in the Rayleigh number. That study also indicated that in the limit of the turbulent Rayleigh number, convective heat transfer is so strong that the temperature change mainly occurs near the wall of the cask, and the natural convection on a local scale plays a more important role than that of global scale. A two dimensional simulation of BWR fuel assembly within a Nitrogen and Helium filled enclosure was done by Araya and Greiner (2007) in an effort to understand the effect on internal convection pattern on overall heat transfer. The study concluded that the effect of natural convection is significant only at lower basket temperatures with Nitrogen backfill, whereas, for Helium backfill, natural convection has negligible impact on overall heat transfer rate. Waturu et al. (2008) performed heat transfer analysis of reinforced concrete storage casks and concrete filled steel casks using the FIT-3D® thermal hydraulics code and the commercial solver PHOENICS®. They compared their computed results with experimental data of Takeda et al. (2008) and the results of their comparison indicate that a hybrid CFD and thermalhydraulic analysis will provide a reasonable



temperature estimate. Lee et al. (2009) performed a detailed experimental and computational analysis of a vertical storage system that was comprised of a stainless steel canister with concrete overpack under both normal and off-normal conditions. The off-normal condition was simulated by blocking the storage system coolant air vent. They demonstrated that the storage cask cooling capacity was adequate for safe operation under both normal and off-normal conditions.

In the present study, the Sierra Nuclear Corporation's ventilated concrete cask-17 (VSC-17) will be used to gain understanding of the spatial temperature distribution in the fuel assembly and other cask components. The description of the cask is provided in later sections. McKinnon et al. (1991) measured temperatures along different cask components that provide a partial understanding of spatial temperature distribution within the cask. The experimental study was later supplemented by a number of computational studies that used thermal-hydraulic codes (McKinnon, 1992) and Computational Fluid Dynamics (CFD) packages (Walavalkar and Schowlater, 2004; Zigh and Solis, 2008, Das et al, 2009). The Computational model developed by Zigh and Solis (2008) that was later used by Das et al. (2009) is adopted in this study to explore the spatial temperature distribution in the VSC-17 storage system components.

Description of the Storage System

The ventilated storage cask system (VSC-17) is a canisterized spent fuel storage system that uses buoyancy driven natural convection as primary mechanism to dissipate decay heat. It has the capacity to store 17 canisters of consolidated nuclear fuel. The VSC-17 system consists of two major components, a multi-assembly sealed basket (MSB) and a ventilated concrete cask (VCC). The MSB has a cylindrical steel vessel that holds an arrangement of guide sleeves. The consolidated fuel assemblies are placed within these guide sleeves. The open MSB cavity is backfilled with either Nitrogen or Helium gas to create an inert atmosphere. A composite shield lid provides sealing to the MSB contents. The sealed MSB is placed within the VCC overpack, with an annular gap between the outer surface of the MSB and inner surface of the VCC. Inlet and outlet opening for this gap is provided through the VCC structure. Coolant air from the surrounding enters the system through an inlet at the bottom, flows vertically upwards as it absorbs thermal energy from the MSB outer surface and exhausts at the top. The VCC is a concrete shell with an inner steel liner and a weather cover. The major components of the VSC-17 storage system are highlighted in Figure 2.1. Detailed configuration geometry and of the system is described in the report of McKinnon et. al. [1992] and McKinnon and DeLoach [1993]



Figure 2.1 may be copyrighted therefore is not included in this notebook. Reference Figure 5-5 from McKinnon, M.A., and DeLoach, V.A., "Spent Nuclear Fuel Storage – Performance Tests and Demonstrations", PNL-8451 and UC-510, April 1993, Pacific Northwest Laboratory, Richland, WA

Figure-2.1 Components of the VSC-17 Dry Storage System (McKinnon and DeLoach 1993)

Computational Thermal Analysis of VSC-17 System

A detailed computational analysis of the VSC-17 cask system was done by CNWRA staff [Das and Basu 2008, Das et al. 2009] and is used in the present study to understand the pattern of spatial temperature distribution. The previous study [Das and Basu, 2008], was based on the computational framework developed for analyzing the VSC-17 cask by Zigh and Solis [2008]. A brief description of the computational techniques and results are discussed in the following section.

Model Development

The commercial CFD package FLUENT® version 6.3 [Fluent, Inc., 2007a] is used in the present analysis. A solution was obtained for the steady-state incompressible Navier-Stokes equations. The pressure based solver of FLUENT® was used in conjunction with a Green-Gauss, cell-based gradient option. An implicit time-marching scheme was used for faster convergence. The SIMPLE algorithm was used to obtain pressure velocity coupling. Details of the governing equations and numerics can be found in FLUENT® theory guide and User's manual [Fluent, Inc., 2007a, b].

A single quadrant of the whole circular cross section of the cask was considered as the computational domain as the heat load distribution is almost same in each quadrant. A symmetry boundary condition was assumed on the quadrant edges. A schematic of the domain and distribution of cross sectional grid in a quadrant is highlighted in Figures 2.2 and 2.3, respectively. The computational domain did not include surrounding ambient environment. The computational grid consisted of 1,038,794 cells and 1,166,560 nodes.



Figure-2.2 Sectional View of VSC-17 Dry Storage System Used in Computation

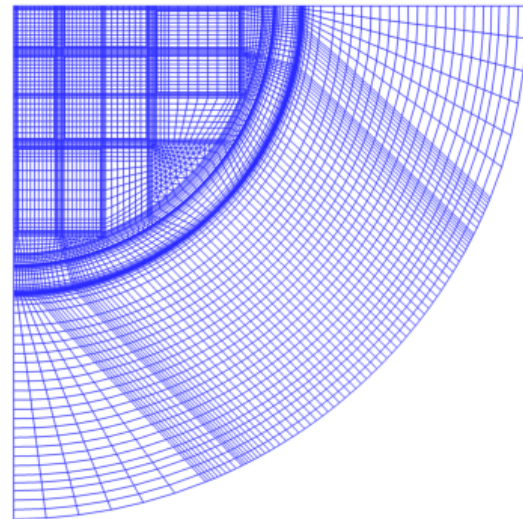


Figure-2.3 Cross Sectional Grid of the Domain

Radiation heat transfer was modeled using the discrete ordinate method. The calculated Reynolds number for the flow was in the transitional range and a number of turbulence model was studied including the standard $k-\omega$ model, the renormalization group $k-\epsilon$ model, the shear stress transport $k-\omega$ model, and the realizable $k-\epsilon$ model. The results presented in the report were generated using the realizable $k-\epsilon$ turbulence model. Convection within the tightly packed consolidated fuel assemblies was neglected. This region was modeled as a homogeneous solid with uniform heat generation. A customized temperature-dependent orthotropic effective thermal conductivity for this region was derived using an auxiliary two-dimensional simulation of an individual fuel assembly. The effective thermal conductivity is used to represent the entire heat transfer by radiation and conduction within this region (Bahney and Lotz 1996). The decay heat value for every fuel assembly that was obtained from experimental observation was applied as a uniform volumetric heat generation rate throughout the homogeneous region; modified only to include an axial power profile based on the measured axial power distribution. Customized user defined functions were used to incorporate the source terms within the CFD solver.

2.1.3.2: Modeling Results



Though the numerical study was conducted for a number of test cases, some sample results are presented in this section to highlight the pattern of temperature distribution within the cask. Results from simulations based on input conditions corresponding to Test #1 of the experimental study [McKinnon, 1992] are presented here. Under this test condition, the MSB cavity was filled with Helium at below atmospheric pressure. No blockages of the inlet or exit air vents were assumed. The computational domain did not include the surrounding atmospheric air and a pressure boundary condition was assumed at the inlet vent.

The temperature contours on different VSC-17 components are shown in Figure 2.4, (a) and (b). It is clear that the fuel basket assembly has considerably higher temperature compared to other components. Peak temperature region within the domain is located approximately near the center of the basket assembly. In the present study, individual fuel rods and claddings were not modeled explicitly. Instead the fuel assembly was treated as a homogeneous solid with uniform heat generation rate with an effective thermal conductivity representing the total heat transfer. Hence, the peak temperature within the basket assembly volume will be used as approximate estimates of cladding surface temperature. The location of the calculated high temperature region is consistent with the experimental observations of McKinnon et al. (1992).

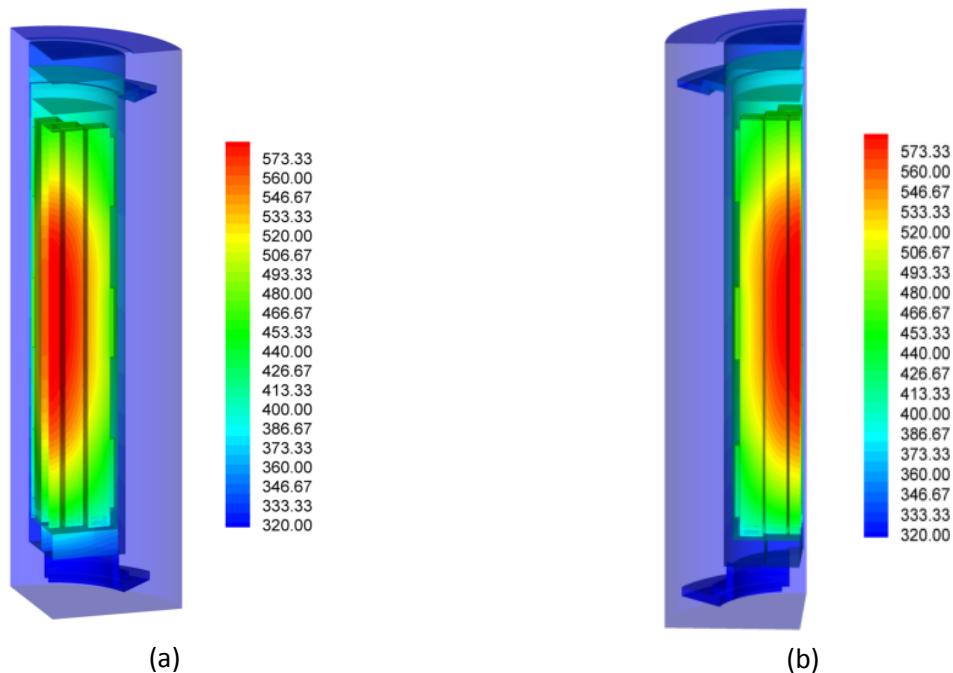


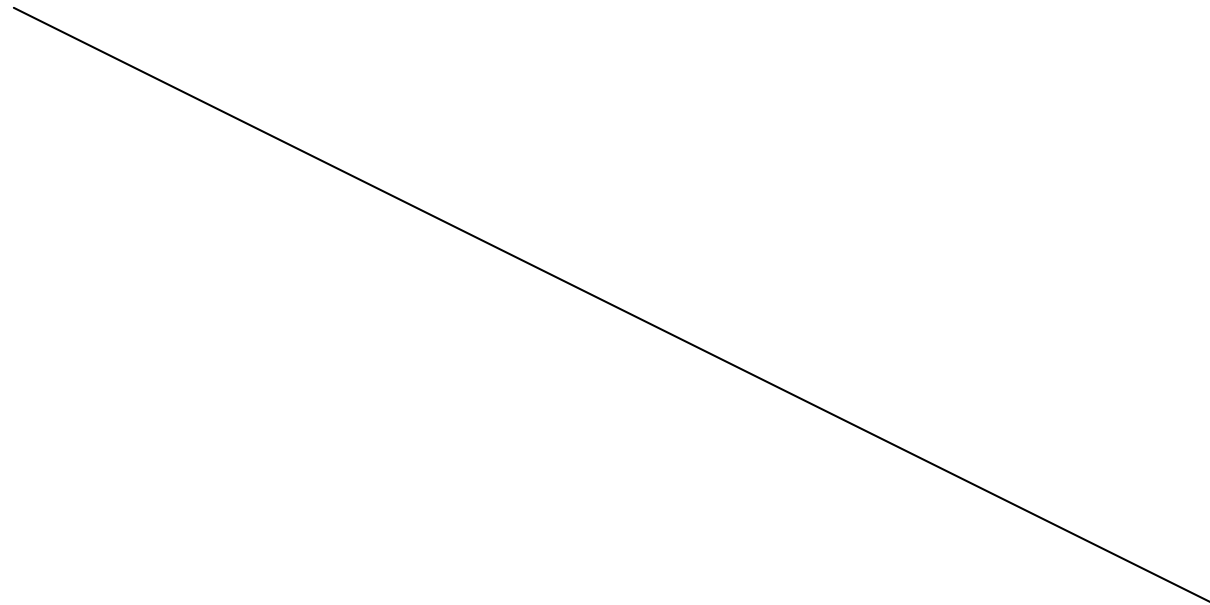
Figure-2.4 Temperature contours (K) in VSC-17 components
[°F = 1.8 °K × -459.4]



The temperature contours for the outside concrete surface and the coolant air flowing through the annular gap between the steel MSB liner and VCC are shown in Figure 2.5. Compared to the temperature of the basket assembly, as shown in Figure 2.4 (a) and (b), the VCC and the air temperature is substantially lower. It can also be observed that the coolant air temperature increases as it flows vertically upwards from inlet to the outlet. The temperature of the outer concrete shell also changes with increased vertical distance.

In the experimental setup (McKinnon 1993), lances with multiple thermocouples were placed at seven different locations along the fuel assembly canisters, that are identified by the lance number. Temperature results along fuel assembly baskets from McKinnon (1993) are reproduced in Figure 2.6 and presented alongside the computed data. At every lance location, the temperature was observed to first increase to a maximum and then decrease with increasing vertical elevation. It can be observed that the peak temperature is slightly overpredicted for all three locations by about 1 to 2 percent; however, the predicted temperature distribution shows qualitative agreement with the experimental data and follows the same pattern and trend.

Computed axial temperature distribution along with experimental data along the steel liner and MPC wall are highlighted in Figure 2.6. Like fuel assembly, computed results overpredict temperature by 5 percent even though the predicted temperature qualitatively agreed with the experimental observations. In general, such deviations between computed and experimental data are attributed to both modeling and parametric uncertainty of the numerical model, as well as to experimental uncertainties. Modeling uncertainties include geometric approximations made to construct the domain and geometry and parametric uncertainties include issues related to material selection and specification of material properties.



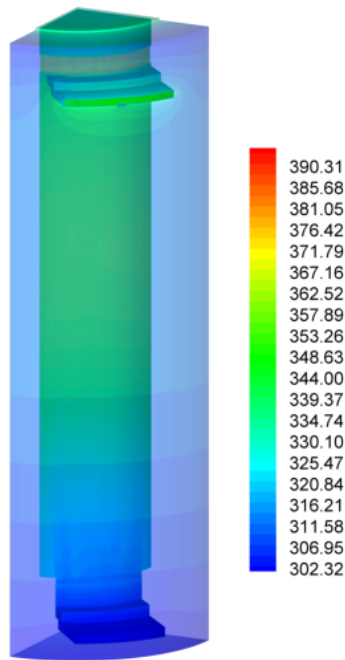


Figure-2.5- Temperature contours (K) in the air passage and concrete shell
[°F = 1.8 °K × -459.4]

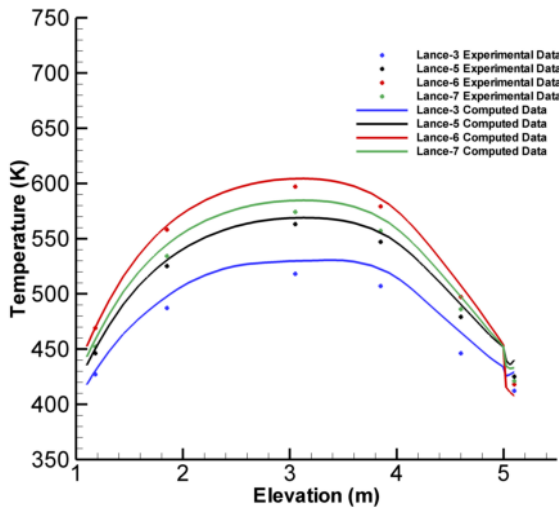


Figure-2.6- Axial Temperature Distribution along the Fuel Assembly Baskets
[°F = 1.8 °K × -459.4]

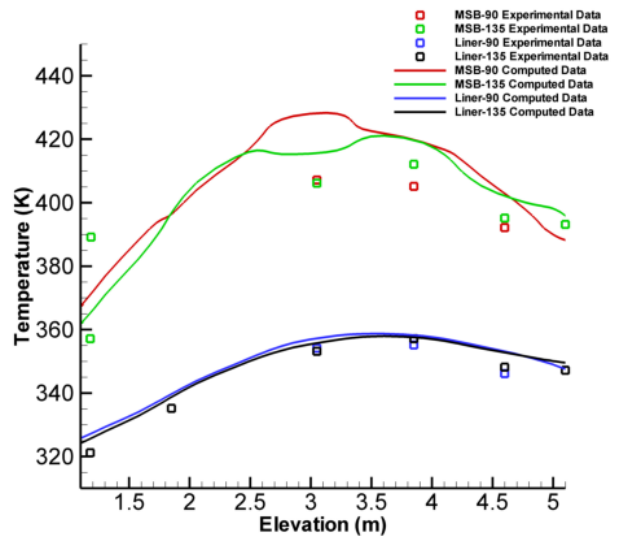


Figure-2.7- Axial Temperature Distribution along the Steel Liner and MPC
[°F = 1.8 °K × -459.4]



Development of Temperature Zones

One of the major focuses of the present study is to understand cladding behavior for extended period of storage. Temperature evolution of cladding surface with time, temperature gradient and time distribution of relative humidity in the MSB cavity provides input required to assess corrosion condition within the storage system. Ideally, a series of quasi-steady numerical simulations with time varying thermal loading, that reflects the decay heat characteristics over the desired period of extended storage, would provide a detailed understanding of the evolving spatial temperature distribution with time. Such an exercise is computationally expensive as a large number of simulations are required to capture the snapshots of changing temperature pattern. As an approximation, in the current study, the detailed simulations described in the previous section are used as the initial estimate of temperature distribution within the VSC-17 system and analytical expressions for temperature evolution from other studies [EPRI, 2002] are adopted to estimate temperature variation with time. This analytical approach, however, is not applied throughout the domain in every computational cell as that would also generate a large quantity of data. Instead, components of interest, such as the fuel assembly, are discretized into a specific number of subvolumes, and the mean temperatures of the subvolumes are used for further analysis. For our study, the fuel assembly zone is divided into five subvolumes based on the temperature range. The computed temperature range (maximum – minimum temperature) in the fuel basket assembly volume is divided into five equal intervals. Sections of the fuel basket assembly volume that have computed temperatures within the same interval are considered to be the part of a same single subvolume. The mean temperature of each range is used as the representative value for that subvolume and for subsequent calculation of time-temperature variation history.

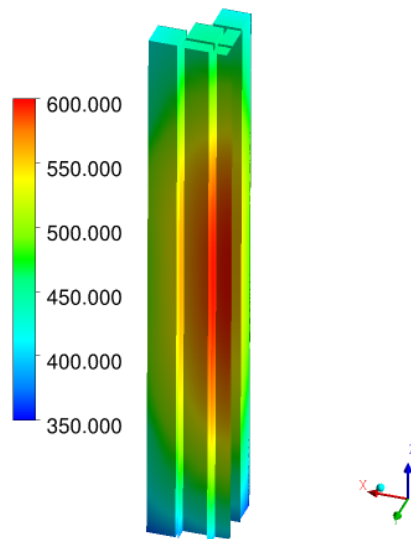


Figure-2.8- Temperature (K) Distribution in the Fuel Assembly Basket
[°F = 1.8 °K × -459.4]



The maximum and minimum temperature within the fuel basket assembly for the VSC-17 cask, under test condition #1 [McKinnon 1992] are 598 K (616.73 oF) and 366 K (199.13 oF), respectively. The general temperature distribution in the basket assembly is shown in Figure 2-8.

As mentioned previously, the temperature range is divided into five equal intervals and any region in the fuel assembly that has temperature within a particular interval is aggregated into a single subvolume and is called a temperature zone. The five temperature zones that were developed for this analysis are shown in Figure 2-9 as viewed from two different directions. Each color band identifies each temperature zone. As can be seen, the lowest temperature zone is at the bottom and the highest temperature zone is location near the center of the fuel assembly.

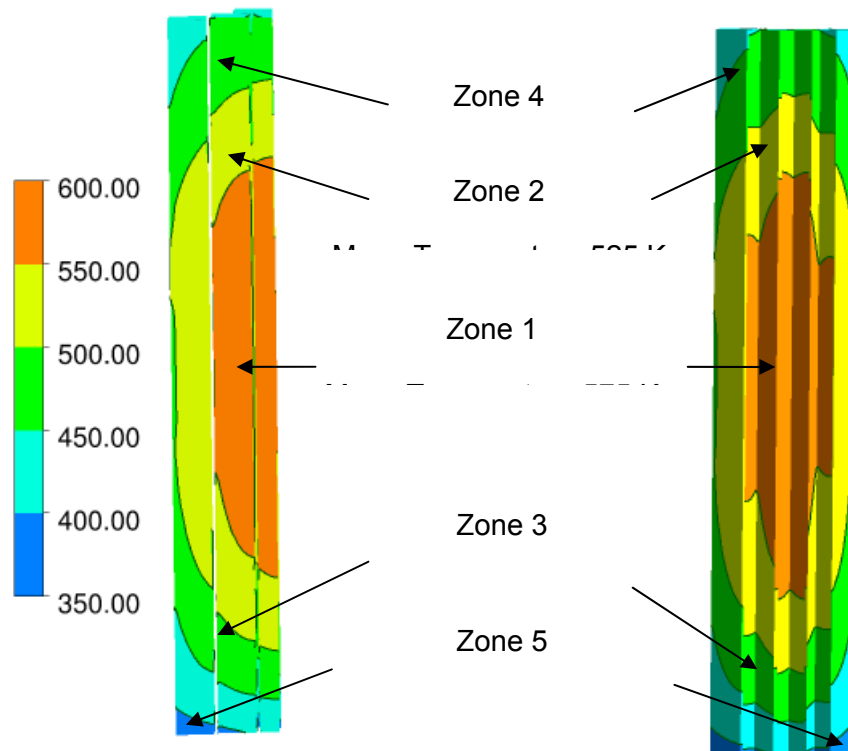


Figure-2.9- Location of the Five Temperature (K) Zones in the Fuel Basket Assembly
[°F = 1.8 °K × -459.4]

The mean temperatures of every temperature zone and approximate percentage of total fuel assembly volume covered by that subvolume is summarized in Table 2.1



| Zone Number | Mean Temperature K [°F] | % of Total Volume |
|-------------|-------------------------|-------------------|
| 1 | 575 [575.3] | 18.95 |
| 2 | 525 [485.3] | 33.00 |
| 3 | 475 [395.3] | 33.72 |
| 4 | 425 [305.3] | 12.38 |
| 5 | 375 [215.3] | 1.95 |

Temperature-time profiles during extended storage

This section describes the study of time evolution of temperature at the five representative temperature zones described previously. The time history has been calculated based on correlations that were obtained from experimental data and fuel characteristics.

11/29/2011

Analytical Expression for Calculating Temperature-Time Variation.

Two bounding estimates of temporal evolution of temperature were proposed as a part of the dry storage characterization project (EPRI, 2002). The (GNS) CASTOR-V/21cask with 15×15 PWR fuel assembly was used for dry storage characterization. A detailed description of the cask is provided in reports of McKinnon [1992] and EPRI [2002]. The CASTOR-V/21cask is a direct-loaded storage system. The main components of this cask include a ductile cast iron cask body, a stainless steel spent fuel basket assembly and stainless steel primary and secondary lids. The cask body is a cylindrical structure of 4.9 m (16 ft) height and 2.4 m (8 ft) in diameter that has 73 heat transfer fins placed circumferentially around the cask. To provide neutron shielding, polyethylene moderator rods are placed within the cask wall body in two concentric rows distributed around the cask perimeter. Two lifting trunnions are bolted on each end of the cask body. The spent fuel basket assembly is made of stainless steel plates and borated stainless steel plate, having a boron content of approximately 1% for criticality control. The basket can hold 21 fuel tubes for storage. A cross sectional view of the cask and the basket assembly are shown in Figures 2-10 and 2-11, respectively. The stainless steel primary lid was sealed using metallic O-rings and 44 bolts. A number of penetrations were made on the primary lid for inserting probes and other devices necessary for the experiment. The stainless steel secondary lid, which is part of the CASTOR V/21 cask was not used during the experimentation, as it was necessary to regularly access the probes and other devices inserted into the system, and not having the secondary lid facilitated access.

For the experiment conducted for the dry storage characterization project, the CASTOR V/21 cask was loaded to its full fuel holding capacity of 21 fuel assemblies. Each assembly contained Westinghouse 15×15 PWR fuel discharged from the Surry reactors of Virginia Power (presently Dominion Power). The burnup of the stored fuel was in the range of 24-35 GWD/MTU and the out-of-reactor cooling period was within 2.2-3.8 years. The per assembly heat load varied



between 1 kW [0.948 BTU/s]] to 1.8 kW [1.71 BTU/s] and the total heat load of the cask was 28.4 kW [26.92 BTU/s].

Detailed spatial temperature measurements were recorded by McKinnon [1992] along the fuel assembly basket for the CASTOR V/21 cask prior to the characterization study. These measurements were recorded using thermocouples that were inserted through the penetrations through the primary lid. At the end of the characterization study, after 14.2 years, another set of temperature measurements were recorded. The measurements were, however, not recorded at the same locations as those made in the initial study and were done with the primary lid open.

| | |
|--|--|
| <p>Figure 2.10 may be copyrighted therefore is not included in this notebook. Reference Figure 1-1 from Electric Power Research Institute, "Dry Cask Storage Characterization Project", Final Report, Report Number 1002882 September, 2002, EPRI, Palo Alto, California</p> | <p>Figure 2.11 may be copyrighted therefore is not included in this notebook. Reference Figure 1-3 from Electric Power Research Institute, "Dry Cask Storage Characterization Project", Final Report, Report Number 1002882 September, 2002, EPRI, Palo Alto, California</p> |
| <p>Figure 2-10: Sectional View of the CASTOR V/21 Cask</p> | <p>Figure 2-11: Sectional View of the Basket Assembly of the CASTOR V/21 Cask</p> |

Two different methods for modeling the temperature profile were developed in the EPRI report (EPRI, 2002) based on the recorded temperatures and fuel characteristics. The first method assumed three temperature points. The initial temperature at time = 0.0 years was fixed at 617 K [650.93 °F], the temperature at the end of cask characterization study at time = 14.8 years was fixed at 428 K [311.54 °F] and it was assumed that at time =100 years, the entire system will be at atmospheric temperature of 311 K [97.45 °F]. The equation obtained using these temperature points was the following

$$T(t) = 308e^{(-0.064 t)} + 309 \quad 2.1$$

where, T is the temperature in Kelvin, t is the time in years.



As the primary lid was open during temperature measurement at the end of the characterization study, after 14.8 years, it was expected that the recorded temperature was lower than the actual temperature within the closed cask. Hence the correlation based on this temperature is used as lower bound of temperature distribution.

The second method was based on the assumption that temperature is first proportional to the exponentially decreasing decay heat and is subsequently dominated by the ambient temperature at later times. As indicated in EPRI (2002), both Cs-137 and Sr-90 are the main contributors for decay heat. For the model expression, the half life of Cs-137 was used as the reference decay heat load since both Cs-137 and Sr-90 have similar half-lives. The initial temperature was fixed at 617 K [650.93 °F]. The analytical expression of temperature profile obtained using this method was the following

$$T(t) = 308 e^{(-0.023 t)} + 309 \quad 2.2$$

As the half life of Cs-137 is longer than that for Sr-90 and was used in deriving equation 2.2, the amount of heat retained in the system will be overestimated. In turn equation 2.2 is expected to bound the actual temperature conditions that were present for the EPRI study. Equation 2.2 is used as the upper bound of temperature distribution in the present assessment.

Assumptions and Modified Equations

Equations 2.1 and 2.2 were derived based on experimental data for CASTOR V/21 cask. A number of assumptions and approximations were made to adopt those equations for the VSC-17 cask, which is being used in the present study. The main assumptions are the listed in the following.

- (a) The temperature distribution within any cask largely depends on the fuel characteristics and the fuel decay heat. As both the CASTOR V/21 and VSC -17 uses 15×15 Westinghouse PWR fuel assemblies, it is assumed that the temporal distribution of temperature within the cask will be analogous. Hence, it is assumed that the temperature of VSC-17 cask components also exhibit the same general pattern of exponential decay as highlighted in equations 2.1 and 2.2. Mathematically it implies that the exponential term in equations 2.1 and 2.2 will remain the same for temperature equations derived for VSC-17.
- (b) For calculating lower bound temperatures, it is assumed that after 100 years of storage, the temperature within the cask will reach the near ambient thermal condition {309 K [96.53 °F]}. Hence the final lower bound temperatures after 100 years are the same for both VSC-17 and CASTOR V/21 casks. The estimated upper temperature bound follows the waste heat decay curve of the fuel and is based on the same assumptions that was used to derive equation 2.2
- (c) The initial temperature used to derive equations 2.1 and 2.2 are fixed at 617 K [650.03 °F]. This is not the case for the present analysis, where different temperature zones in VSC-17 fuel assembly will have different initial temperatures. Hence, equations 2.1 and 2.2 are modified to accommodate the difference in initial temperatures. Equations are



adjusted so that initial temperature difference decreases exponentially with time. Furthermore, it is assumed that the decay in this temperature difference is similar to the decay in temperature, i.e. the same exponential decay constants are used for calculating the decay in temperature difference.

The modified equation for the lower bound of temperature is provided by

$$T(t) = (T_{\text{mean}} - 309)e^{(-0.064 t)} + 309 \quad 2.3$$

where, T_{mean} is the mean temperature (K) of a temperature zone.

Similarly, the modified equations for the upper bound temperature is derived from equation 2.2 and is given by

$$T(t) = (T_{\text{mean}} - 309)e^{(-0.023 t)} + 309 \quad 2.4$$

Results of Time-Temperature History

Figure 2-12 shows the lower bound temperature for all the temperature zones listed in Table 2.1. As can be seen in the Figure, the temperatures decrease exponentially over the time frame considered, when it reaches the ambient temperature of 311 K [97.45 °F]. It can also be observed that the temporal gradient of temperature increases with increased initial temperature. As a result, the zone-1 temperature distribution curve is steeper for the first hundred years as compared to zone-5. This can be attributed to the fact that the equations 2.3 and 2.4 were developed with an approximation that a fixed temperature at the end of 100 years will be attained by all the components. In actual storage devices, it is likely that different temperature zones will reach the ambient condition at different point of time, with the hottest region attaining the atmospheric temperature at the end. Hence, the slopes of the temperature curves will likely be more uniform. Figure 2-13 shows the upper temperature bounds for different zones using equation 2.4. The upper bound temperature curves show similar pattern and distribution as highlighted in Figure 2-12 for lower bound temperatures.

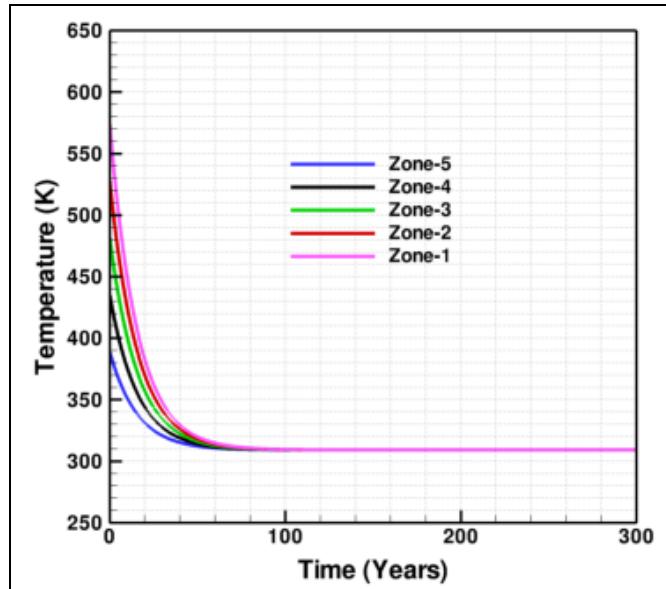


Figure 2-12 Lower Bound of Temperature at Different Temperature Zones
[°F = 1.8 °K × -459.4]

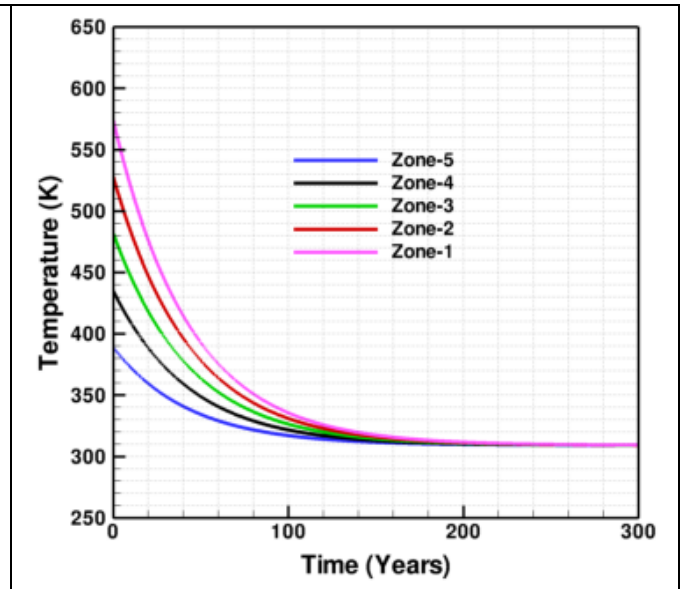


Figure 2-13 Upper Bound of Temperature at Different Temperature Zones
[°F = 1.8 °K × -459.4]

12/1/2011

Relative humidity profile

Due to imperfect and incomplete drying, some residual water may remain within the canister. At relatively high temperatures, this residual water will remain in vapor state. As temperature starts to decrease, relative humidity within the container starts to increase. If temperature of any surface within the container drops below the saturation temperature, the local relative humidity will be at 100% and water vapor will condense to form liquid water on that surface.

In the present study, the time evolutions of relative humidity and condensation within the sealed canister of the VSC-17 system have been investigated. The study has not considered detailed spatial movement of water vapor within the canister cavity and localized condensation on every internal surface. Instead, an analytical approach is developed to estimate the local relative humidity and condensation rate using the mean temperatures for the five zones listed in Table 2.1.

Assumptions and Approximations

A number of approximations and assumptions are made in these studies and are listed in the following.

- (a) The internal open volume of the canister cavity is fixed at 2.33 m³ [82.28 ft³]. The total volume occupied by other significant components such as the fuel assembly basket was deducted from the total cavity volume. This value is approximate as some of the smaller components such as steel support beams were not considered in the volume calculation.



- (b) A lumped parameter approach is adopted for analytical formulation and spatial distribution of temperature within the volume is not considered.
- (c) The fluid inside the canister was assumed to be a binary mixture of the backfill gas and water vapor. It was assumed that any non-condensable component of the backfill gas, if present, does not affect condensation.
- (d) An equilibrium condition was assumed within the system. This means that when the enclosed volume reached a relative humidity of 100%, any water that would have caused supersaturation of the fluid will completely condense to form liquid water.
- (e) Most of the results presented in the report assume that that 55 moles of water remained in the canister due to incomplete drying. A parametric study has been done to assess the effect of initial water mass on the system.
- (f) The analysis has been done for each of the five temperature zones in isolation. This means that the mean temperature of each temperature zone and its variation with time is used to calculate the relative humidity in its vicinity. In this isolated analysis, it is also assumed that the entire mass of water vapor is in contact with the surface and is available for condensation.
- (g) The analytical study for calculating relative humidity presented in this section does not consider any other mass transfer process, other than condensation. Hence, processes such as radiolysis and corrosion are initially not considered and are incorporated later in the report.
- (h) Pressure remains the same after condensation. This essentially means that the water vapor only exerts a minor fraction of the total pressure and the mass of water vapor is insignificant. This may need further revision if there is a significant quantity of water.
- (i) The gas temperature is assumed to be not affected by condensation, as the phase change heat transfer takes place only at the wall. This is a reasonable assumption as the thermal mass of the wall is higher compared to the gas mass.

Analytical Expressions for Calculating Relative Humidity and Condensation

Relative humidity is calculated using the following equation

$$RH = 100 \times \frac{P_{vp}(T)}{P_{vp,sat}(T)} \quad 2.5$$

where, RH is the relative humidity, $P_{vp}(T)$ is the partial pressure of water vapor at the temperature (T), and $P_{vp,sat}(T)$ is the saturation vapor pressure of water vapor at the temperature (T)

The saturation vapor pressure as a function of temperature can be obtained using the following relationship [Kennan et al 1997]



$$P_{v,sat}(T_C) = 217.99 \times e^{\left[\frac{0.01}{273.15+T_C} (374.136-T_C) \sum_{k=0}^7 F_k (0.65-0.01T_C)^k \right]}$$

2.6

where,

$$\begin{aligned} F_0 &= -741.9242, \\ F_1 &= -29.721, \\ F_2 &= -11.55286, \\ F_3 &= -0.8685635, \\ F_4 &= 0.1094098, \\ F_5 &= 0.439993, \\ F_6 &= 0.2520658, \\ F_7 &= 0.05218684, \end{aligned}$$

$P_{v,sat}$ is the water vapor saturation pressure in atmosphere [1 atmosphere = 14.7 psi], and T_C is the temperature in °C.

The temperature range of validity for the above mentioned equation is 0°C to 374°C. The main reason for choosing this relationship is that it is valid for the temperature range that is expected in a normally functioning cask over time. The primary interest is the temperature range when condensation is likely to happen, which is within the validity limit of the cask system. The variation of saturation vapor pressure with temperature within 350°C and 600°C is highlighted in Figure 2-14 .

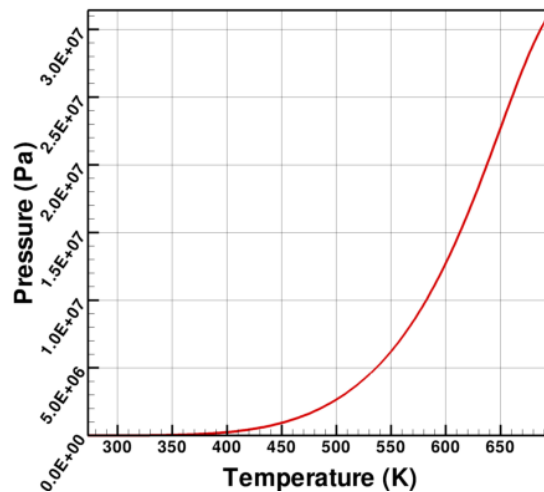


Figure 2-14: Variation of Saturation Vapor Pressure with Temperature
[1 Pa = 1.45×10^{-4} psi; °F = 1.8 °K × -459.4]

At any point of time, the condensate mass was calculated using the following equation



$$n_{cond}(t) = n(t) - n_{sat}(T) \quad 2.7$$

where, $n_{cond}(t)$ is the amount of condensate water mass at time t in moles, $n(t)$ is the amount of water vapor at that point of time (t) in moles, and $n_{sat}(T)$ saturation mole fraction at temperature T .

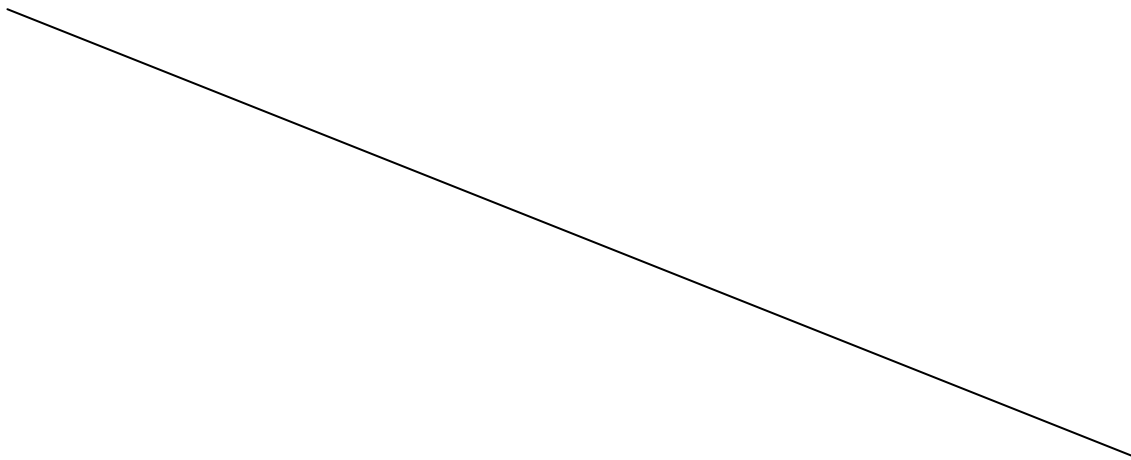
The number of moles of water vapor in saturation condition at temperature T can be calculated using the expression:

$$n_{sat}(T) = \frac{P_{vp,sat}(T) \times V}{RT} \quad 2.8$$

where, V is the open cavity volume and R is the universal gas constant. Any water present in excess to that will have to be condensed in order to maintain equilibrium. The equations above will give an idea about the water vapor remaining in the system. Once it reaches the saturation limit, the water vapor content will remain at the saturation value.

Results of Relative Humidity and Condensation

The relative humidity calculated using the analytical expressions provided in equations 2.6 and 2.7 are shown in Figures 2-15 and 2-16. Figure 2-15 and 2-16 shows the time variation of relative humidity for the lower bound and upper bounds of temperature estimates, respectively. As can be seen, the calculated time to reach saturation (100% relative humidity) is shorter, when the lower bound temperatures are used in the computation as compared to upper bound temperatures. This is expected, as the lower bound temperature equation predicts a faster decay in temperature and the saturation temperature is encountered early in the time-temperature curve.



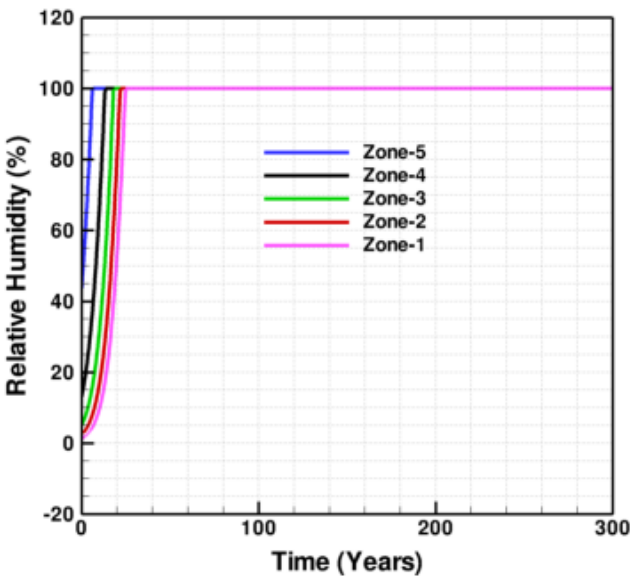


Figure 2-15 Relative Humidity for Different Temperature Zones with Lower Bound of Temperatures

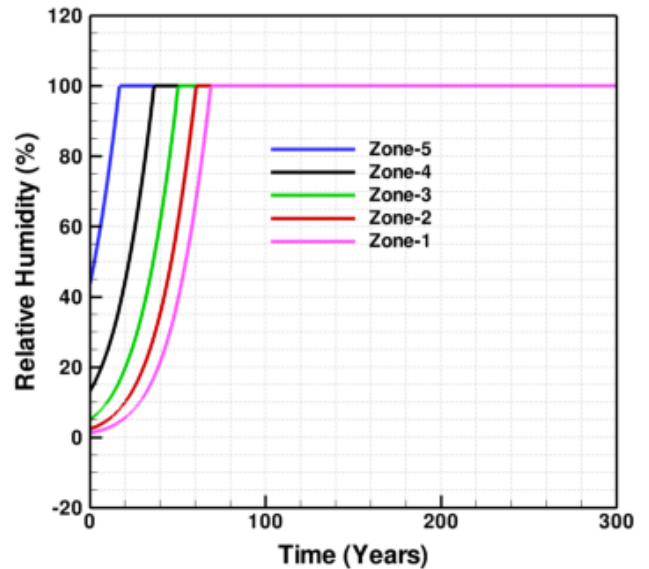


Figure 2-16 Relative Humidity for Different Temperature Zones with Upper Bound of Temperatures

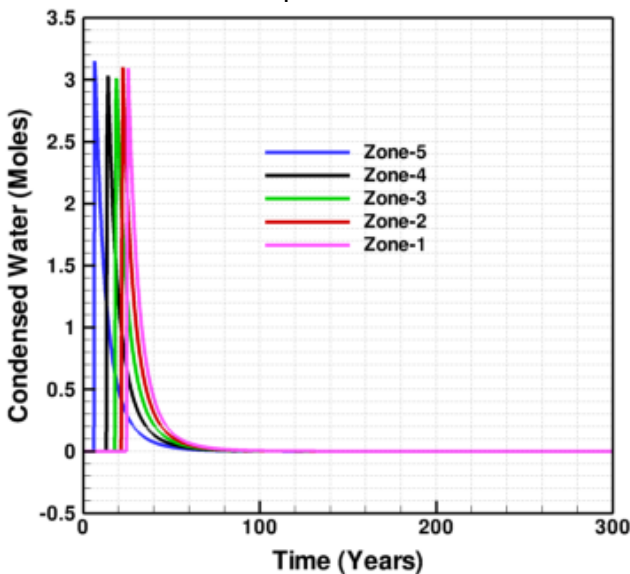


Figure 2-17 Mass of Condensed Water Calculated Using Lower Bound of Temperatures

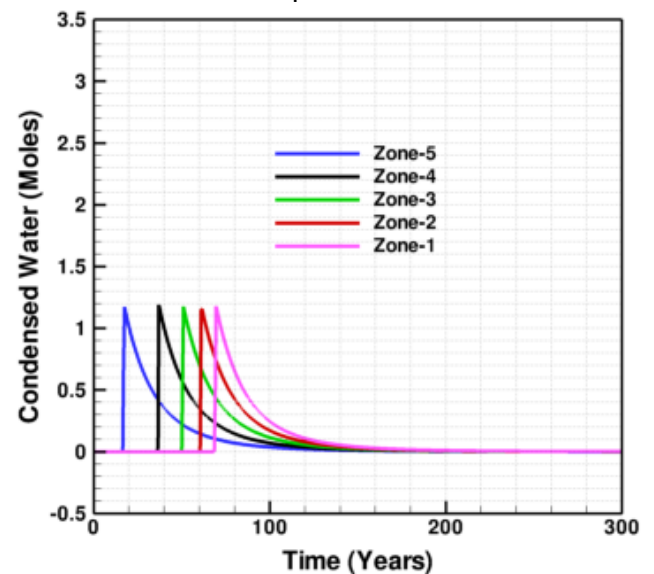


Figure 2-18 Mass of Condensed Water Calculated Using Upper Bound of Temperatures

The time variation of condensed water mass calculated using the lower and upper bound temperature estimates for all five temperature zones are shown in Figures 2-17 and 2-18, respectively. In general, the pattern of condensation rate is similar for all the surfaces, and expectedly the condensation starts early on relatively cooler surfaces (zone-5) as compared to relatively hotter surfaces (zone-1). This is because the temperature of the cooler surfaces reaches the saturation temperature sooner compared to the hotter surfaces. Similarly, on the same surface, early condensation is predicted by the lower bound temperature estimates as



compared to upper bound temperature estimates. This can also be attributed to the fact that the lower bound temperature equation predicts the onset of saturation early. A comparison between Figures 2-17 and 2-18 also shows that when the lower temperature bound is used in the calculation; the predicted peak condensation rate is high, but the overall condensation process occurs for a shorter duration. The difference in the condensation rate reflects the difference in the temperature gradient between the lower and upper temperature bounds as highlighted in Figures 2-12 and 2-13.

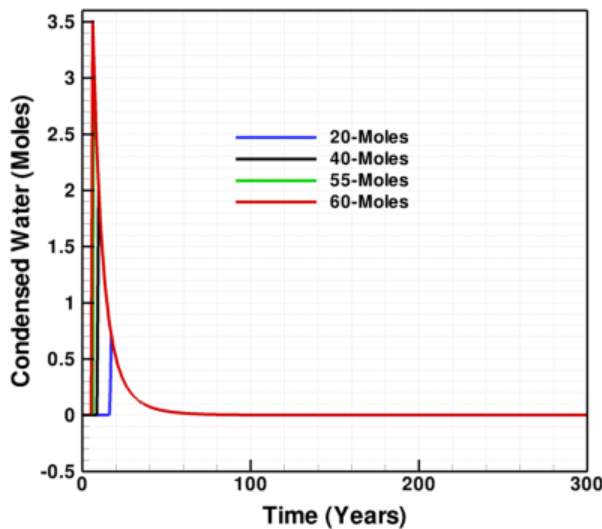


Figure 2-19 Effect of the Initial Water Mass on Condensation; Calculation Used Lower Bound of Temperatures

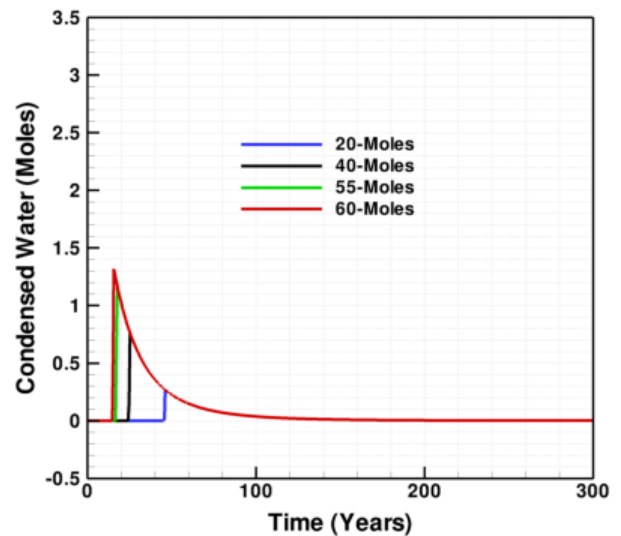


Figure 2-20 Effect of the Initial Water Mass on Condensation; Calculation Used Upper Bound of Temperatures

As mentioned in previously, it is assumed that 55 moles of water vapor will remain in the canister cavity due to incomplete drying. It is recognized that the initial moisture mass will vary depending on drying efficiency. As a result, a parametric study was carried out to understand the effect of variable initial water mass on condensation rates. Figures 2-19 and 2-20 show the distribution of condensate formation on temperature zone-5, with four different initial conditions of water mass in the canister calculated using low and high temperature bounds. It is clear that rate of condensation increases with increased initial water content. This is due to the fact that all the systems studied has the same internal pressure, thus condensation rate becomes only a function of available water vapor mass. It can also be noted that the time when condensation initiates is also dependent on the initial moisture content. The pressure within the cavity is constant and the temperature decay is same for all the systems. Under this circumstance, inception of saturation condition is determined by the moisture content. As a result, systems with higher initial moisture content will reach saturation point early compared to systems that have a lower level of initial moisture content.



12/5/2011

Available water profile considering other physical processes

Apart from condensation, a number of other physical processes such as radiolysis significantly impact the environment within the storage canister. These processes can use existing water mass and chemically convert water and decomposition products to other compounds and at the same time can recombine those compounds to create water that is added back to the existing mass of water.

Assumptions and Approximations

There are a few assumptions made in deriving the analytical expression for calculating water used in different physical processes and the subsequent variation in relative humidity profiles. The main process that consumes water is radiolysis. It is assumed that radiolysis takes precedence over condensation. Therefore at any point of time; water is allowed to be radiolyzed first and the remaining mass of water is allowed to be condensed if the environment is conducive for condensation. It was also assumed that radiolysis process ceased to progress once the water content was consumed. In addition, all the assumptions listed in connection with calculating relative humidity and condensation also applies for the calculations performed in this section.

Analytical Expressions for Calculating Radiolysis

Four different equations were formulated to assess water retained in the system after radiolysis. A discussion of the assumptions used for accounting for radiolysis and chemical kinetics and deriving the expressions is presented in other chapter. The first set of two equations provided the lower and upper bounds of water consumption due to radiolysis and is shown in equations 2.9 and 2.10 respectively. These equations were derived assuming an exponential reaction rate.

$$m(t) = m_0 e^{(-1.92904 t)} \quad 2.9$$

$$m(t) = m_0 e^{(-0.128609 t)} \quad 2.10$$

where, $m(t)$ is the water mass left in the system after radiolysis at any time t ,
 m_0 is the initial water mass, and t is the time in years.

The second set of two equations was derived assuming a linear rate of water consumption. The upper and lower bound estimates for the water mass are provided in equations 2.11 and 2.12 respectively

$$m(t) = m_0 - 11.5282 \times t \quad 2.11$$



$$m(t) = m_0 - 0.767883 \times t$$

2.12

2.3.3 Results of Internal Cask Environment Considering Radiolysis

Relative humidity calculations considering radiolysis are presented in this section. Calculations were performed for temperature zone-1, which has the highest initial temperature and it is expected that the other temperature zones will exhibit similar trend.

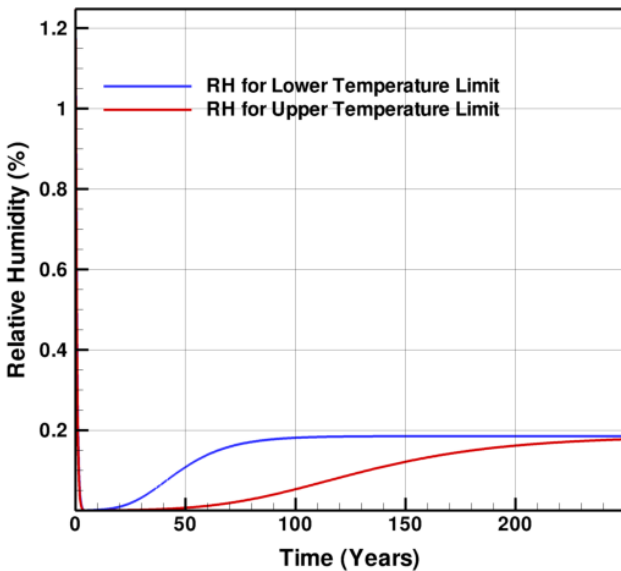


Figure 2-21 Relative Humidity Distribution Using Equation 2.9 (Exponential Decay Upper Bound) for the Upper and Lower Bound of Temperature

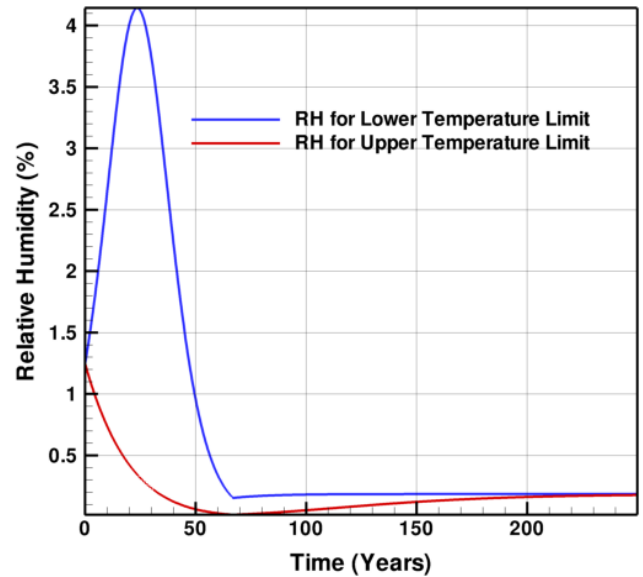


Figure 2-22 Relative Humidity Distribution Using Equation 2.10 (Exponential Decay Lower Bound) for the Upper and Lower Bound of Temperature

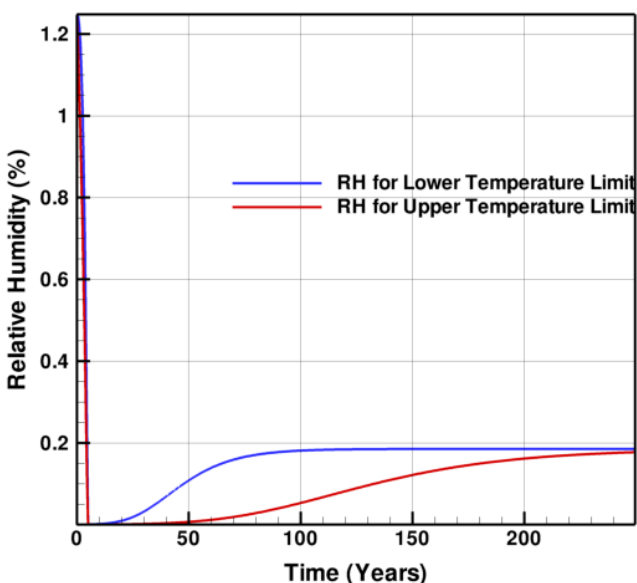


Figure 2-23 Relative Humidity Distribution Using Equation 2.11 (Linear Decay Upper Bound) for the Upper and Lower Bound of Temperature

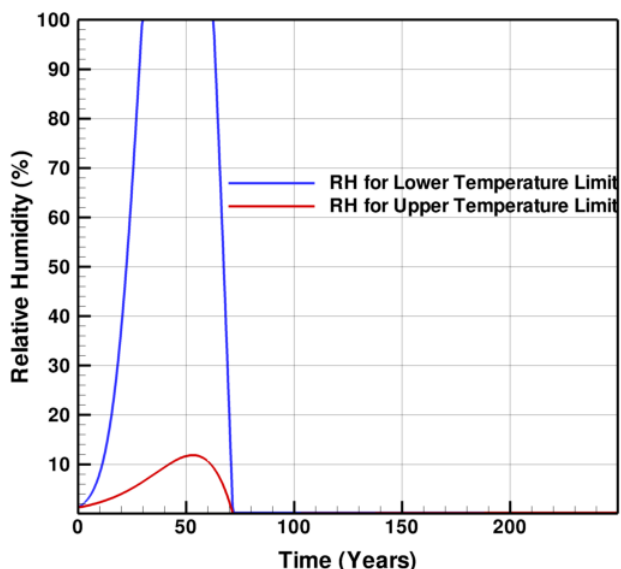


Figure 2-24 Relative Humidity Distribution Using Equation 2.12 (Linear Decay Lower Bound) for the Upper and Lower Bound of Temperature

The variation of relative humidity calculated using the upper and lower bounds of exponential reaction rates are shown in Figures 2-21 and 2-22, respectively. The red curve in each figure was obtained using the upper temperature limit and the blue curve was obtained using the lower temperature limit. It can be seen that relative humidity drops rapidly within the first three years and never goes beyond 5%. After a steep initial drop, relative humidity rises slightly and remains steady for the rest of the storage period. This phenomenon is the artifact of the assumption that radiolysis stops when the mass of residual moisture is consumed. The slight increase in humidity is a result of this residual moisture that is assumed to be present in the system. These results also show that if radiolysis dominates the mass transfer process early in the system, when condensation is not significant and later when the temperature drops substantially, there is not enough water vapor left to saturate the system.

The variation in relative humidity calculated using the upper and lower bounds of linear reaction rates are shown in Figures 2-23 and 2-24, respectively. The results for the upper bound is similar to that obtained using the exponential distribution and highlighted in Figures 2-22 and 2-23. For this scenario, the relative humidity drops rapidly and the subsequent increase in RH is due to the near zero residual moisture content, which is assumed in the calculation. In essence, the radiolysis consumes almost all the available moisture within a short duration of time. Figure 2-24, however, shows that for the lower temperature bound, saturation condition exists in the system for a short duration. This is due to the fact that in this scenario the radiolysis process was relatively slow and there were enough moisture left in the system to saturate it. As the radiolysis proceeded further, more water was consumed and the system became undersaturated that is evidenced by a drop of relative humidity from its peak value of 100%. This observation in Figure 2-25 indicates that when the radiolysis is slow, there exists a possibility of condensation.



References

Araya, P.E. and Greiner, M. "Two-Dimensional Simulations of Natural Convection/Radiation Heat Transfer for BWR Assembly within Isothermal Enclosure", Packaging, Transport, Storage and Security of Radioactive Materials, Vo. 18(3), pp. 171-179, 2007

Arya, M. S., Keyhani, M., "Convective heat transfer in a sealed storage cask containing spent-fuel canisters", Nuclear Science and Engineering, Vol. 105, pp. 391-403.

Bahney, R.H. and T.L. Lotz. "Spent Nuclear Fuel Effective Thermal Conductivity Report." Las Vegas, Nevada: TRW Environmental Safety Systems, Inc. 1996.

Bare, W.C., and Torgerson, L.D., "Dry Cask Storage Characterization Project- Phase I: CASTOR V/21 Cask Opening And Examination" INEEL/EXT-01-00183, 2001, Idaho National Engineering and Environmental Laboratory, Idaho Falls, Idaho 83415

Cannan, R. E., Klein, D. E., "A numerical investigation of natural convection heat transfer within horizontal spent-fuel assemblies", Nuclear Technology, Vol. 123, pp. 193-208.

Das, K., Basu, D., and Axler, K., "Validation Of Modeling Approach to Evaluate Transportation, Aging, and Disposal Canister Thermal Designs", CNWRA, November, 2008, San Antonio, TX

Das, K, Basu, D, Solis, J, and Zigh, Z, "Computational Fluid Dynamics Modeling Approach to Evaluate VSC-17 Dry Storage Cask Thermal Designs", CFD4NRS-3, Experimental Validation and Application of CFD and CMFD Codes to Nuclear Reactor Safety Issues 14-16 September 2010, Washington, DC, USA

Electric Power Research Institute, "Dry Cask Storage Characterization Project", Final Report, September, 2002, EPRI, Palo Alto, California

Fluent, Inc., "FLUENT® Theory Guide Version 6.3," Lebanon, New Hampshire: Fluent, Inc. (2007a).

Fluent, Inc., "FLUENT® User Manual Version 6.3," Lebanon, New Hampshire: Fluent, Inc. (2007b).

Heng, X., Zuying, G., and Zhiwei, Z., "A numerical investigation of natural convection heat transfer in horizontal spent-fuel storage cask", Nuclear Engineering and Design, Vol. 213, pp. 59-65, 2002

Keenan, J. H., Keyes, F. G., Hill, P. G., Moore, J. G., Steam Tables: Thermodynamic Properties of Water, Including Vapor, Liquid, and Solid Phases, John Wiley and Sons, Inc, 1969. As cited in Chapter 5 of ASHRAE Handbook and Product Directory, 1977 Fundamentals, Third Printing,



American Society of Heating Refrigeration and Air Conditioning Engineers, Inc., New York, p. 5.12.

Lee, J.C, Choi, W.S., Bang, K.S. Seo, K.S. and Yoo, S.Y., "Thermal-Fluid Flow Analysis and Demonstration Test of a Spent Fuel Storage System", Nuclear Engineering and Design Vol. 239, pp. 551-558, 2009

Lombardo, N.J., J. M. Cuta, T.E. Michener, D. R. Recot and C.L. Wheeler, "COBRA-SFS: A Thermal Hydraulic Analysis Computer Code, Volume-III: Validation Assessments", PNL-6049, UC-85, December 1986, Pacific Northwest Laboratory, Richland, WA

McCann, R.A. and P.S. Lowery, "HYDRA-II: A Hydrothermal Analysis Computer Code Volume-III: Verification and Validation Assessments", PNL-6206, UC-85, October 1987, Pacific Northwest Laboratory, Richland, WA

McKinnon, M. A., Dodge, R. E., Schmitt, R. C., Eslinger, L. E., and Dineen, G., "Performance Testing and Analyses of the VSC-17 Ventilated Concrete Cask," TR-100305, Electric Power Research Institute, Palo Alto, California, 1992.

McKinnon, M.A., and DeLoach, V.A., "Spent Nuclear Fuel Storage – Performance Tests and Demonstrations", PNL-8451 and UC-510, April 1993, Pacific Northwest Laboratory, Richland, WA

McKinnon, M.A., "Spent Fuel Integrity during Dry Storage", Institute of Nuclear Materials Management 36th Annual Meeting July 9-12, 1995 Palm Desert, California

McKinnon, M.A., and Doherty A. L., "Spent Nuclear Fuel Storage – Performance Tests and Demonstrations", PNNL-11576 and UC-810, June 1997, Pacific Northwest Laboratory, Richland, WA

Takeda, H., M. Wataru, K. Shirai, T. Saegusa, "Heat Removal Verification Tests Using Concrete Casks Under Normal Condition", Nuclear Engineering and Design, Vol. 238, pp. 1196-1205, 2008.

Walavalkar, A.Y., D.G. Schowalter, "3-D CFD Simulation of a Spent Nuclear Fuel Storage System," American Nuclear Society, Vol. 19, pp. 200–201 (2004).

Wataru, M., H. Takeda, K Shirai, T. Saegusa, "Thermal Hydraulic Analysis Compared with Tests of Full Scale Concrete Casks", Nuclear Engineering and Design, Vol. 238, pp. 1213-1219, 2008.

Zigh, G, and Solis, J., "Computational Fluid Dynamics Best Practice Guidelines in the Analysis of Storage Dry Casks", Waste Management 2008 Symposia, February 24-28, 2008, Phoenix, AZ.



Suggestions of Subsequent Work

1. The spatial variation of temperature was calculated using a correlation that was derived for a different cask. For proper estimate of temperature, numerical simulations should be performed for the entire storage period. This can be accomplished by doing a finite number of quasi-steady simulations at different time points, where the input thermal load in the canister is obtained from the decay curve. The results obtained from these snapshot simulations will provide a comprehensive idea about the time distribution of temperature within the cask.
2. The relative humidity and condensation calculation has to be carried out in conjunction with the thermal calculations described above. The moisture distribution within the canister cavity is highly dependent on local thermodynamic condition and a conjugate simulation will provide the needed understanding of the moisture propagation and condensation within the system.
3. Other associated processes such as radiolysis and corrosion that significantly affects the moisture content within the canister should also be considered within any simulation exercise describe above.
4. For canisterized storage system such as VSC-17, corrosion of canister outer surface will depend on a number of external factors such as salt deposition especially in a marine environment. The computational framework described in this report can be extended to include the propagation of these species through the coolant channels and subsequent deposition on the outer surface.



12/12/2011

Location of the program in the server Niagra and in the attached electronic media

1. The general directory /ext-storage: Contains all the files related to basic study and initial calculation related to temperature and relative humidity calculation. The program "humidity-3.f" was used to generate the results. Tecplot-2009 layout files are available in this directory
2. The baseline directory ext-storage also has two EXCEL files. VSC-17-data.xlsx has all the files that contain the VSC-17 related data for zonal distribution and mean temperatures
3. The directory /ext-storage/vsc-17/ has the basic study related to condensation evaporation and temperature calculation for the VSC-17 cask. The program humidity-4.f is the code used to calculate and generate data. This program considers radiolysis as a water consumption mechanism.
4. The directory /ext-storage/vsc-17/temperature-study contain files related to temperature and relative humidity calculation for the VSC-17 cask. This program calculates the relative humidity without consideration of radiolysis. The program here is humidity-no-radiolysis.f. All the input data files and Tecplot files are available in this directory.
5. The directory /ext-storage/vsc-17/clip-data contain simulation files for CFD analysis of VSC-17 cask. The run condition for this simulation corresponds to the test condition #1 in the experiment of McKinnon. The state files for CFD-Post and corresponding contour diagrams are provided in this directory. The simulation case and data files were taken from the previous study of Das (2008) and were not regenerated for the present project.

12/14/2011

The temperature calculations were performed the five temperature zones were created for a single time point. The temperature distribution inside the cask will vary with time and the relative extent of every temperature zone will also change with time. This in turn will change the relative humidity and condensation rates within each zone. Presently, the time variation of temperature is estimated using an empirical correlation assuming that the extend of each temperature zone is fixed. For a more detail and accurate understanding of time-temperature-relative humidity history, numerical simulations should be carried out for the entire period of extended storage that accounts for the decay heat load. This can be accomplished by doing a finite number of quasi-steady simulations at different time points, where the input thermal load in the canister is obtained from the decay curve. The results obtained from these snapshot simulations will provide a comprehensive idea about the variation of temperature and the temperature zones along with spatial distribution of relative humidity and condensation.



Modification of section 2.1.3.3

2.1.3.3: Development of Temperature Zones

One of the major focuses of the present study is to understand cladding behavior for extended period of storage. Temperature evolution of cladding surface with time, temperature gradient and time distribution of relative humidity in the MSB cavity provides input required to assess corrosion condition within the storage system. Ideally, a series of quasi-steady numerical simulations with time varying thermal loading, that reflects the decay heat characteristics over the desired period of extended storage, would provide a detailed understanding of the evolving spatial temperature distribution with time. Such an exercise is computationally expensive as a large number of simulations are required to capture the snapshots of changing temperature pattern. As an approximation, in the current study, the detailed simulations described in the previous section are used as the initial estimate of temperature distribution within the VSC-17 system and analytical expressions for temperature evolution from other studies [EPRI, 2002] are adopted to estimate temperature variation with time. This analytical approach, however, is not applied throughout the domain in every computational cell as that would also generate a large quantity of data. Instead, components of interest, such as the fuel assembly, are discretized into a specific number of subvolumes, and the mean temperatures of the subvolumes are used for further analysis. For our study, the fuel assembly zone is divided into five subvolumes based on the temperature range. The computed temperature range (maximum – minimum temperature) in the fuel basket assembly volume is divided into five equal intervals. Sections of the fuel basket assembly volume that have computed temperatures within the same interval are considered to be the part of a same single subvolume. The mean temperature of each range is used as the representative value for that subvolume and for subsequent calculation of time-temperature variation history.

The maximum and minimum temperature within the fuel basket assembly for the VSC-17 cask, under test condition #1 [McKinnon 1992] are 598 K (616.73 °F) and 366 K (199.13 °F), respectively. The general temperature distribution in the basket assembly is shown in Figure 2-8.

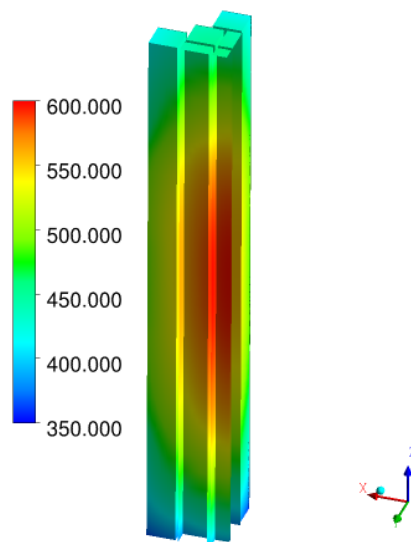


Figure-2.8- Temperature (K) Distribution in the Fuel Assembly Basket
[°F = 1.8 °K × -459.4]

As mentioned previously, the temperature range is divided into five equal intervals and any region in the fuel assembly that has temperature within a particular interval is aggregated into a single subvolume and is called a temperature zone. The five temperature zones that were developed for this analysis are shown in Figure 2-9 as viewed from two different directions. Each color band identifies each temperature zone. As can be seen, the lowest temperature zone is at the bottom and the highest temperature zone is located near the center of the fuel assembly. The zonal temperature distributions based on the CFD calculation are treated as the lower initial temperature limit.

The temperature computations were done for a single time step and for a single set of fuel heat load. It is recognized that changing the fuel heat load will change the temperature zones and the mean temperatures. The maximum temperature of the hottest zone, however, should not exceed the allowable fuel cladding temperature of 673 K [751.7° F]. An upper limit of initial temperature distribution for every zone was develop, by arbitrarily increasing the highest temperature of the hottest central zone was to the maximum allowable limit and adjusting the temperature of the other zones accordingly. This was done to parametrically study the effect of temperature variation within each zone. It should, however, be noted that the relative extend of each temperature zones were not changed.

The mean initial high and low temperatures of every temperature zone and approximate percentage of total fuel assembly volume covered by that subvolume is summarized in Table 2.1

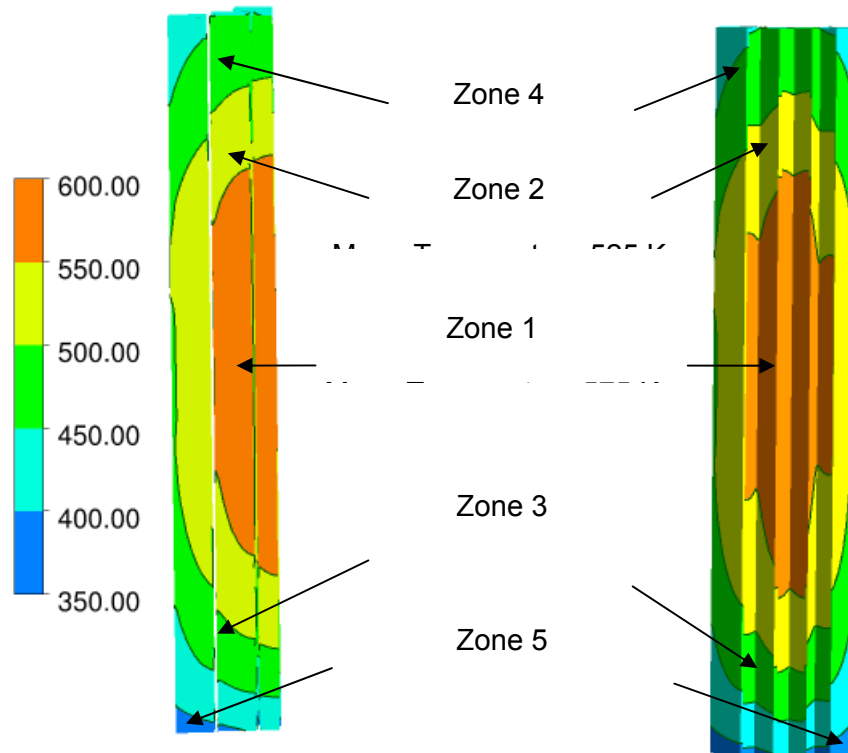


Figure 2-9. Location of the Five Temperature (K) Zones in the Fuel Basket Assembly
[°F = 1.8 °K × (-459.4)]

| Table 2.1 Mean Temperatures and Percentage of Volume of Five Temperature Zones | | | |
|--|--|---|-------------------|
| Zone Number | Low-end Fuel and Cladding Initial Temperature K [°F] | High-end Fuel and Cladding Initial Temperature K [°F] | % of Total Volume |
| 1 | 575 [575.3] | 673 [751.7] | 18.95 |
| 2 | 525 [485.3] | 623 [661.7] | 33.00 |
| 3 | 475 [395.3] | 573 [571.7] | 33.72 |
| 4 | 425 [305.3] | 523 [481.7] | 12.38 |
| 5 | 375 [215.3] | 481 [406.1] | 1.95 |



1/3/13

The attached CD contains all the electronic files developed for the analysis. The FORTAN code humidity-3.f was used to calculate the temperature distribution, water content and relative humidity data. The directory vsc-17 contains all the analysis that is specific to VSC-17 cask.

Note: Some of the figures and data used in this notebook are proprietary.

Correction: 5/13/2013: Sources of the figures were researched and it was found that they are not proprietary but may be copyrighted. Kaushik Das



Appendix-A

Programs used to calculate the temperature, relative humidity and condensation rate without considering radiolysis

```
c23456789
C edited on 10/10/11
c Temperature and Relative Humidity Calculation
c*****

      real rgas      ! gas constant
      real nw_h     ! Number of moles of water high temperature
      real nw_l     ! Number of moles of water low temperature
      real nw_ini   ! Number of moles of water initially present
      real nw_sat
      real nw_cond
      real MW_Water

      dimension nw_h(5000)
      dimension nw_l(5000)

      nw_ini = 60.0
      vol = 2.33 ! Open volume within the cask (2.33)
      rgas = 8.314 ! R in J/K-mole
      MW_Water = 18.0/1000. !Molar Weight of Water kg/mole

c Initial temperature differences as correction

      t_vsc = 389.0 ! VSC-17 initial temperature in Kelvin
      t_castor = 617.0 ! CASTOR V/21 initial temperature in Kelvin
      tdiff = t_vsc - t_castor ! correction term for correlations
      write(*,*) ' The correction temperature is ', tdiff, ' C'

      dt = 0.5 ! Time step size in years
      t0 = 0.0 ! Start Time
      tf = 300.0 ! End time
      N = ifix((tf-t0)/dt) ! Number of time steps
      write(*,*) 'Time step size in years=',dt
      write(*,*) 'End time=',tf
      write(*,*) 'Number of time steps=',N

      open(unit=20,file='temp-humidity.dat')
      write(20,*) 'Title=Temperature-Humidity-Data'
      write(20,*) 'variables=Time,Temperature,Relative-Humidity,Water-
&content,Condensed-water-moles,Condensed-water-kg'

c Lower temperature limit loop

      write(20,*) 'zone T= "Lower-Limit", i=',N,',f=point'
      nw_h(1) = nw_ini
      do i=1,N
      time= t0+ dt*(float(i-1)) ! Time in years
      temp = 308.0*exp(-0.064*time)+309 + tdiff*exp(-0.064*time)
```



```

! Temperature in K
rad1 = nw_ini*exp(-1.92904*time)
rad2 = nw_ini*exp(-0.128609*time)
rad3 = nw_ini - 11.5182*time
rad4 = nw_ini - 0.767883*time
rad = rad4
if (rad.le.0.01) then
  rad = 0.01
endif
c   nw_h(i)= rad

write(*,*) 'time, rad, remaining=',time, rad,
&   nw_ini*exp(-1.92904*time)

pvp = nw_h(i)*rgas*temp/vol      ! Partial pressure of WV
psat = fpsat(temp)              ! Saturation Vapor Pressure
rh = pvp*100.0/psat
if (rh.gt.100.0) then
  rh = 100.0
  nw_sat = psat*vol/(rgas*temp)
  nw_cond = nw_h(i) - nw_sat
else
  nw_cond = 0.0
endif
nw_h(i+1) = nw_h(i)-nw_cond
w_cond = nw_cond*MW_water
write(20,*) time,temp,rh,nw_h(i),nw_cond,w_cond
enddo
write(*,*) 'Lower Temperature Loop Calculation End'

c Upper temperature limit loop

write(20,*) 'zone T= "Upper-Limit", i=',N,',f=point'
nw_l(1) = nw_ini
do i=1,N
time= t0+ dt*(float(i-1))      ! Time in years
temp = 308.0*exp(-0.023*time)+309 + tdiff*exp(-0.023*time)
! Temperature in K

rad1 = nw_ini*exp(-1.92904*time)
rad2 = nw_ini*exp(-0.128609*time)
rad3 = nw_ini - 11.5182*time
rad4 = nw_ini - 0.767883*time
rad = rad4
if (rad.le.0.01) then
  rad = 0.01
endif
c   nw_l(i)= rad

write(*,*) 'time, rad, remaining=',time, rad,
&   nw_ini*exp(-1.92904*time)

pvp = nw_l(i)*rgas*temp/vol      ! Partial pressure of WV
psat = fpsat(temp)              ! Saturation Vapor Pressure
c   write(*,*) 'temp=',temp,' pvp=',pvp,' psat= ',psat
rh = pvp*100.0/psat
if (rh.gt.100.0) then

```



```
rh = 100.0
nw_sat = psat*vol/(rgas*temp)
nw_cond = nw_l(i) - nw_sat
else
nw_cond = 0.0
endif
nw_l(i+1) = nw_l(i)-nw_cond
w_cond = nw_cond*MW_water
write(20,*) time,temp,rh,nw_l(i),nw_cond,w_cond
enddo
write(*,*) 'Upper Temperature Loop Calculation End'

close(20)
stop
end
```

```
function fpsat(temp2)
dimension f(8)
f(1)=-741.9242
f(2)=-29.721
f(3)=-11.55286
f(4)=-0.8685635
f(5)=0.1094098
f(6)=0.439993
f(7)=0.2520658
f(8)=0.005218684
tc=temp2-273.0 ! Temperature in deg C
total=0.0
do i= 1,8
total = total + f(i)*((0.65-0.01*tc)**(i-1))
enddo
term=0.01*(374.136-tc)/(273.15+tc)
fpsat=101325.0*217.99*exp(term*total)
return
end
```




Programs used to calculate the temperature, relative humidity and condensation rate considering radiolysis

```

c23456789
C edited on 10/10/11
c Temperature and Relative Humidity Calculation
c*****

      real rgas    ! gas constant
      real nw_h   ! Number of moles of water high temperature
      real nw_l   ! Number of moles of water low temperature
      real nw_ini  ! Number of moles of water initially present
      real nw_sat
      real nw_cond
      real MW_Water

      dimension nw_h(5000)
      dimension nw_l(5000)

      nw_ini = 55.0
      vol = 2.33    ! Open volume within the cask (2.33)
      rgas = 8.314 ! R in J/K-mole
      MW_Water = 18.0/1000. !Molar Weight of Water kg/mole

c Initial temperature differences as correction

      t_vsc = 574.0 ! VSC-17 initial temperature in Kelvin
      t_castor = 617.0 ! CASTOR V/21 initial temperature in Kelvin
      tdiff = t_vsc - t_castor ! correction term for correlations
      write(*,*) ' The correction temperature is ', tdiff, ' C'

      dt = 0.5    ! Time step size in years
      t0 = 0.0    ! Start Time
      tf = 250.0  ! End time
      N = ifix((tf-t0)/dt) ! Number of time steps
      write(*,*) 'Time step size in years=',dt
      write(*,*) 'End time=',tf
      write(*,*) 'Number of time steps=',N

      open(unit=20,file='temp-humidity.dat')
      write(20,*) 'Title=Temperature-Humidity-Data'
      write(20,*) 'variables=Time,Temperature,Relative-Humidity,Water-
&content,Condensed-water-moles,Condensed-water-kg'

c Lower temperature limit loop

      write(20,*) 'zone T= "Lower-Limit", i=',N,',f=point'
      nw_h(1) = nw_ini
      do i=1,N
      time= t0+ dt*(float(i-1))           ! Time in years
      temp = 308.0*exp(-0.064*time)+309 + tdiff*exp(-0.064*time)
                                           ! Temperature in K

      rad1 = nw_ini*exp(-1.92904*time)
      rad2 = nw_ini*exp(-0.128609*time)
      rad3 = nw_ini - 11.5182*time
      rad4 = nw_ini - 0.767883*time

```



```

    rad = rad4
    if (rad.le.0.01) then
        rad = 0.01
    endif
    nw_h(i)= rad

    write(*,*) 'time, rad, remaining=',time, rad,
&          nw_ini*exp(-1.92904*time)

    pvp = nw_h(i)*rgas*temp/vol          ! Partial pressure of WV
    psat = fpsat(temp)                  ! Saturation Vapor Pressure
    rh = pvp*100.0/psat
    if (rh.gt.100.0) then
        rh = 100.0
        nw_sat = psat*vol/(rgas*temp)
        nw_cond = nw_h(i) - nw_sat
    else
        nw_cond = 0.0
    endif
    nw_h(i+1) = nw_h(i)-nw_cond
    w_cond = nw_cond*MW_water
    write(20,*) time,temp,rh,nw_h(i),nw_cond,w_cond
    enddo
    write(*,*) 'Lower Temperature Loop Calculation End'

c Upper temperature limit loop

    write(20,*) 'zone T= "Upper-Limit", i=',N,',f=point'
    nw_l(1) = nw_ini
    do i=1,N
        time= t0+ dt*(float(i-1))          ! Time in years
        temp = 308.0*exp(-0.023*time)+309 + tdiff*exp(-0.023*time)
            ! Temperature in K

        rad1 = nw_ini*exp(-1.92904*time)
        rad2 = nw_ini*exp(-0.128609*time)
        rad3 = nw_ini - 11.5182*time
        rad4 = nw_ini - 0.767883*time
        rad = rad4
    if (rad.le.0.01) then
        rad = 0.01
    endif
    nw_l(i)= rad

    write(*,*) 'time, rad, remaining=',time, rad,
&          nw_ini*exp(-1.92904*time)

    pvp = nw_l(i)*rgas*temp/vol          ! Partial pressure of WV
    psat = fpsat(temp)                  ! Saturation Vapor Pressure
c    write(*,*) 'temp=',temp,' pvp=',pvp,' psat= ',psat
    rh = pvp*100.0/psat
    if (rh.gt.100.0) then
        rh = 100.0
        nw_sat = psat*vol/(rgas*temp)
        nw_cond = nw_l(i) - nw_sat
    else
        nw_cond = 0.0

```



```
endif
nw_l(i+1) = nw_l(i)-nw_cond
w_cond = nw_cond*MW_water
write(20,*) time,temp,rh,nw_l(i),nw_cond,w_cond
enddo
write(*,*) 'Upper Temperature Loop Calculation End'

close(20)
stop
end
```

```
function fpsat(temp2)
dimension f(8)
f(1)=-741.9242
f(2)=-29.721
f(3)=-11.55286
f(4)=-0.8685635
f(5)=0.1094098
f(6)=0.439993
f(7)=0.2520658
f(8)=0.005218684
tc=temp2-273.0 ! Temperature in deg C
total=0.0
do i= 1,8
total = total + f(i)*((0.65-0.01*tc)**(i-1))
enddo
term=0.01*(374.136-tc)/(273.15+tc)
fpsat=101325.0*217.99*exp(term*total)
return
end
```

ADDITIONAL INFORMATION FOR SCIENTIFIC NOTEBOOK NO. 1087E

| | |
|--|---|
| Document Date: | 7/20/2011 |
| Availability: | Southwest Research Institute® Center for Nuclear Waste Regulatory Analyses 6220 Culebra Road San Antonio, Texas 78228 |
| Contact: | Southwest Research Institute® Center for Nuclear Waste Regulatory Analyses 6220 Culebra Road San Antonio, TX 78228-5166 Attn.: Director of Administration 210.522.5054 |
| Data Sensitivity: | <input type="checkbox"/> "Non-Sensitive" <input type="checkbox"/> Sensitive <input checked="" type="checkbox"/> "Non-Sensitive - Copyright" <input type="checkbox"/> Sensitive - Copyright |
| Date Generated: | 4/5/2012 |
| Operating System: (including version number) | Windows |
| Application Used: (including version number) | |
| Media Type: (CDs, 3 1/2, 5 1/4 disks, etc.) | CD |
| File Types: (.exe, .bat, .zip, etc.) | Out file, PNG image, Dat File, and Lay File |
| Remarks : (computer runs, etc.) | Notebook supplemental material |



GEOSCIENCES AND ENGINEERING DIVISION

SCIENTIFIC NOTEBOOK REVIEW CHECKLIST RECORD

Scientific Notebook No. 1087E Project Numbers: 20.14010.01.002

Accomplished

- GW 1. Initial entries per QAP-001
- GW 2. Dating of entries
- NA 3. Corrections (crossed out, one line through w/initials/date)
- GW 4. No white out used
- GW 5. Page number visible on copy or original notebook
- GW 6. In process entries per QAP-001
- GW 7. Figure information present
- GW 8. Text readable
- GW 9. Blank pages and blank portions of pages have a diagonal line to prevent unauthorized future entries.
- GW 10. Permanent ink or type only
- GW 11. Signing of entries (not required on each page)
- GW 12. Electronic media in the scientific notebook properly labeled
- GW 13. Copyrighted or proprietary material fully referenced

Any discrepancies must be resolved before notebook closeout.

I have reviewed this scientific notebook and find it in agreement with QAP001.

Andreas Wittmayer
 Manager Signature

1/21/2013
 Date

~~ESN is labeled proprietary because of creek design information.~~
 These is no proprietary information in this scientific notebook.

Andreas Wittmayer
 5/10/2013